NASA/TP—2014-216633

Liquid Oxygen Thermodynamic Vent System Testing With Helium Pressurization

Neil T. Van Dresar
Glenn Research Center, Cleveland, Ohio

April 2014

NASA STI Program . . . in Profile

Since its founding, NASA has been dedicated to the advancement of aeronautics and space science. The NASA Scientific and Technical Information (STI) program plays a key part in helping NASA maintain this important role.

The NASA STI Program operates under the auspices of the Agency Chief Information Officer. It collects, organizes, provides for archiving, and disseminates NASA's STI. The NASA STI program provides access to the NASA Aeronautics and Space Database and its public interface, the NASA Technical Reports Server, thus providing one of the largest collections of aeronautical and space science STI in the world. Results are published in both non-NASA channels and by NASA in the NASA STI Report Series, which includes the following report types:

- TECHNICAL PUBLICATION. Reports of completed research or a major significant phase of research that present the results of NASA programs and include extensive data or theoretical analysis. Includes compilations of significant scientific and technical data and information deemed to be of continuing reference value. NASA counterpart of peer-reviewed formal professional papers but has less stringent limitations on manuscript length and extent of graphic presentations.

- TECHNICAL MEMORANDUM. Scientific and technical findings that are preliminary or of specialized interest, e.g., quick release reports, working papers, and bibliographies that contain minimal annotation. Does not contain extensive analysis.

- CONTRACTOR REPORT. Scientific and technical findings by NASA-sponsored contractors and grantees.

- CONFERENCE PUBLICATION. Collected papers from scientific and technical conferences, symposia, seminars, or other meetings sponsored or cosponsored by NASA.

- SPECIAL PUBLICATION. Scientific, technical, or historical information from NASA programs, projects, and missions, often concerned with subjects having substantial public interest.

- TECHNICAL TRANSLATION. English-language translations of foreign scientific and technical material pertinent to NASA's mission.

Specialized services also include creating custom thesauri, building customized databases, organizing and publishing research results.

For more information about the NASA STI program, see the following:

- Access the NASA STI program home page at *http://www.sti.nasa.gov*

- E-mail your question to *help@sti.nasa.gov*

- Fax your question to the NASA STI Information Desk at 443–757–5803

- Phone the NASA STI Information Desk at 443–757–5802

- Write to:
  STI Information Desk
  NASA Center for AeroSpace Information
  7115 Standard Drive
  Hanover, MD 21076–1320

NASA/TP—2014-216633

Liquid Oxygen Thermodynamic Vent System Testing With Helium Pressurization

Neil T. Van Dresar
Glenn Research Center, Cleveland, Ohio

National Aeronautics and
Space Administration

Glenn Research Center
Cleveland, Ohio 44135

April 2014

Acknowledgments

Funding was provided by the Propulsion and Cryogenic Advanced Development (PCAD) Project. The author gratefully recognizes the outstanding support provided by the entire test facility team of operations engineers and technicians at the Creek Road Cryogenic Complex, the test hardware design engineers, and the data system programmers at the NASA Glenn Research Center.

Level of Review: This material has been technically reviewed by expert reviewer(s).

Available from

NASA Center for Aerospace Information
7115 Standard Drive
Hanover, MD 21076–1320

National Technical Information Service
5301 Shawnee Road
Alexandria, VA 22312

Available electronically at http://www.sti.nasa.gov

Contents

Liquid Oxygen Thermodynamic Vent System Testing With Helium Pressurization

Neil T. Van Dresar
National Aeronautics and Space Administration
Glenn Research Center
Cleveland, Ohio 44135

Summary

This report presents the results of several thermodynamic vent system (TVS) tests with liquid oxygen plus a test with liquid nitrogen. In all tests, the liquid was heated above its normal boiling point to 111 K for oxygen and 100 K for nitrogen. The elevated temperature was representative of tank conditions for a candidate lunar lander ascent stage.

An initial test series was conducted with saturated oxygen liquid and vapor at 0.6 MPa. The initial series was followed by tests where the test tank was pressurized with gaseous helium to 1.4 to 1.6 MPa. For these tests, the helium mole fraction in the ullage was quite high, about 0.57 to 0.62.

TVS behavior is different when helium is present than when helium is absent. The tank pressure becomes the sum of the vapor pressure and the partial pressure of helium. Therefore, tank pressure depends not only on temperature, as is the case for a pure liquid-vapor system, but also on helium density (i.e., the mass of helium divided by the ullage volume). Thus, properly controlling TVS operation is more challenging with helium pressurization than without helium pressurization.

When helium was present, the liquid temperature would rise with each successive TVS cycle if tank pressure was kept within a constant control band. Alternatively, if the liquid temperature was maintained within a constant TVS control band, the tank pressure would drop with each TVS cycle. The final test series, which was conducted with liquid nitrogen pressurized with helium, demonstrated simultaneous pressure and temperature control during TVS operation. The simultaneous control was achieved by systematic injection of additional helium during each TVS cycle. Adding helium maintained the helium partial pressure as the liquid volume decreased because of TVS operation.

The TVS demonstrations with liquid oxygen pressurized with helium were conducted with three different fluid-mixer configurations—a submerged axial jet mixer, a pair of spray hoops in the tank ullage, and combined use of the axial jet and spray hoops. A submerged liquid pump and compact heat exchanger located inside the test tank were used with all the mixer configurations. The initial series without helium and the final series with liquid nitrogen both used the axial jet mixer. The axial jet configuration successfully demonstrated the ability to control tank pressure; but in the normal-gravity environment, the temperature in the upper tank region (ullage and unwetted wall) was not controlled. The spray hoops and axial jet combination also successfully demonstrated pressure control as well as temperature control of the entire tank and contents. The spray-hoops-only configuration was not expected to be a reliable means of tank mixing because there was no direct means to produce liquid circulation. However, surprisingly good results also were obtained with the spray-hoops-only configuration (i.e., performance metrics such as cycle-averaged vent flowrate were similar to those obtained with the other configurations).

A simple thermodynamic model was developed that correctly predicted the TVS behavior (temperature rise or pressure drop per TVS cycle) when helium was present in the ullage. The model predictions were correlated over a range of input parameters. The correlations show that temperature rise or pressure drop per cycle was proportional to both helium mole fraction and tank heat input. The response also depended on the tank fill fraction: the temperature rise or pressure drop (per TVS cycle) increased as the ullage volume decreased.

1.0 Background

The thermodynamic vent system (TVS) is a technology developed to control the tank pressure of subcritical cryogenic propellant tanks in low-gravity (low-Bond-number) environments where surface tension strongly affects liquid position. Because of their cold temperature and volatility, cryogenic liquids will inevitably absorb thermal energy from the surroundings and build up pressure in a closed vessel. In a normal- or reduced-gravity (such as on the Moon) environment, or if the liquid is settled by thrusting, conventional practice is to control pressure by venting vapor directly from the ullage as needed. For a given pressure (between the triple and critical points), a unique saturation temperature exists. Therefore, controlling tank pressure also maintains the liquid propellant in a saturated condition at the corresponding temperature. In a microgravity environment, it may not be possible to directly vent the ullage vapor with confidence because the liquid position within the propellant tank cannot be predicted with certainty. Furthermore, it may be undesirable to consume propellant to settle the liquid in the tank and enable direct ullage venting. The TVS is a proposed alternative method for controlling tank pressure in microgravity.

With a TVS, a small quantity of sacrificial liquid is removed from the propellant tank: that is, it is vaporized and then vented from the tank. As depicted in Figure 1, liquid is withdrawn from the propellant tank and expanded through a Joule-Thomson (J–T) device to a lower pressure, becoming a two-phase mixture of liquid and vapor at a lower temperature. (In microgravity, a liquid acquisition device would be needed to extract liquid from the tank.) The two-phase mixture is then passed through the cold side of a heat exchanger, absorbing heat and vaporizing completely. The vapor is then vented to the external environment, generally space vacuum. Meanwhile, a second liquid flow is drawn from the tank and pumped through the warm side of the heat exchanger where thermal energy is removed from the flow. The cooled liquid is then returned to the tank and mixed with the tank's contents. The mixing action is driven by various methods, such as axial jets or spray devices.

A properly designed mixing system should at least produce uniform temperatures throughout the liquid region in the tank or perhaps the entire tank volume. Generally, a TVS is more efficient when operated intermittently because pump operation dissipates additional energy into the tank at a significantly greater rate than the environmental heating rate of the tank. In addition, when the TVS is operating, the pressure reduction rate is larger than the tank's self-pressurization rate. Such a system with a liquid pump, known as an active TVS, is the subject of this report. An alternative design without a pump to circulate the liquid inside the tank is known as a passive TVS.

Figure 2 illustrates typical tank pressure and temperature behavior during cyclic TVS operation. When the pressure is near the lower set point, the fluid is well mixed and isothermal. In the absence of helium pressurant gas, the minimum temperature corresponds to the saturation temperature at the lower set-point pressure. However, when the pressure is near the upper set point, the tank has been in a quiescent state for a long period and the fluid is most likely thermally stratified. Because the fluid temperature is not uniform, there is no longer a straightforward connection between the tank pressure and temperature. (In normal gravity, the liquid free surface is at the saturation temperature corresponding to the tank pressure, whereas the liquid below the free surface is subcooled and the vapor above is superheated.)

A TVS also can be used to control temperature and pressure in a tank pressurized with gaseous helium (GHe). Two key differences that affect the behavior of a GHe-pressurized system in comparison to a tank containing only liquid propellant and its vapor should be recognized. First, with noncondensable GHe present, the total tank pressure is the sum of the vapor pressure of the propellant and the partial pressure of the GHe. Therefore, the total tank pressure and the propellant temperature are decoupled. The liquid is subcooled with respect to the total tank pressure. The second difference is that

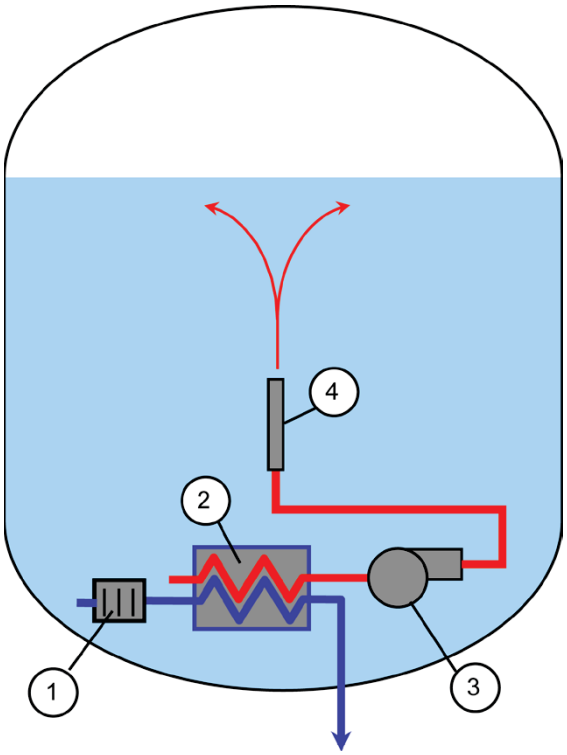

Figure 1.—Simplified schematic of thermodynamic vent system (TVS) hardware: 1—Joule-Thomson device, 2—Heat exchanger, 3—Liquid recirculation pump, 4—Axial jet (or alternatively, a spray bar).

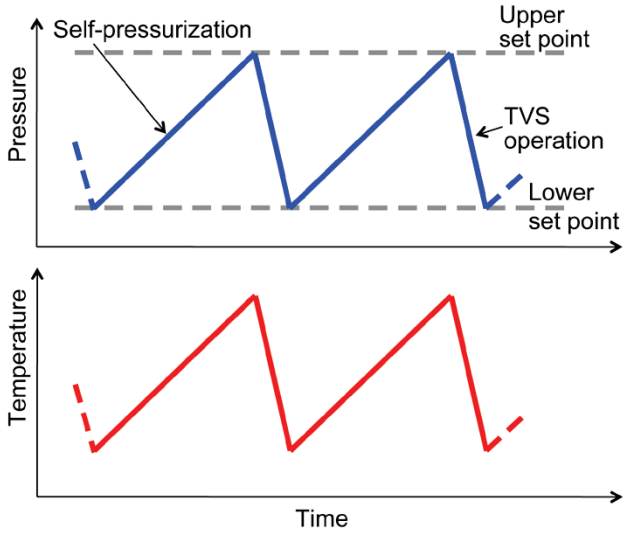

Figure 2.—Idealized thermodynamic vent system (TVS) operational control for a system of pure liquid propellant and its vapor.

the mass of GHe in the ullage remains constant (assuming that no GHe is added to the tank and neglecting GHe dissolution in the liquid). As TVS cycles progress, liquid is removed from the tank and the ullage volume increases. Therefore, the GHe density decreases with each successive TVS cycle. The effects of having GHe in the ullage are discussed in greater detail in Section 1.1 and several other sections.

For a tank that contains only liquid propellant and its vapor and that is subjected to pressure control by either ullage venting or TVS operation, liquid temperature can only be maintained at the saturation temperature corresponding to the tank pressure. If the tank is pressurized with GHe, ullage venting reduces pressure, but at the expense of some GHe loss. When the GHe is completely removed by venting, the liquid is at the saturation temperature corresponding to the tank pressure. A TVS allows pressure reduction and temperature control without the loss of GHe.

1.1 Previous Thermodynamic Vent System Testing

Most of NASA's documented TVS experimentation has been conducted at the NASA Marshall Flight Center using liquid hydrogen (LH_2), liquid nitrogen (LN_2), and liquid methane (LCH_4) (Refs. 1 to 5). Early testing was conducted primarily with pure propellant vapor in the tank ullage (Refs. 1 and 2), but later tests placed a greater emphasis on conditions involving GHe as a pressurant gas (Refs. 3 to 5). The test hardware for the Marshall tests consisted of an 18.09-m^3 cylindrical test tank with elliptical ends. A combined spray bar and concentric tube heat exchanger assembly was oriented vertically within the tank near the tank's central axis. The liquid recirculation pump and J–T valve(s) were located outside of the test tank for easier accessibility.

In the tests with pure propellant vapor in the ullage, the TVS concept was demonstrated to successfully maintain tank pressure between the lower and upper set points, typically using a control bandwidth of about 3 or 6 kPa. Nominal test pressures were from 118 to 138 kPa. The maximum operating pressure for the Marshall test tank was 344 kPa. Testing with noncondensable pressurant gas (helium) has been limited mostly to relatively low GHe mole fractions in the ullage (estimated to be 5 to 27 percent), generally because of maximum test pressure limitations.

Of particular interest to the current work is the TVS testing done with LCH_4 and GHe pressurization (Ref. 4). In all of the Marshall tests, the total test pressure was limited by the test tank's operational limit and generally the use of GHe pressurization was limited to low mole fractions of GHe in the ullage. However, in the LCH_4 test, the vapor pressure was lowered (by subcooling the liquid) to 56 to 70 kPa in comparison to the near-normal boiling point at atmospheric pressure (~100 kPa) for the other tests. The low vapor pressure allowed for a significantly greater GHe mole fraction in the ullage—estimated to be 60 to 65 mol%. The liquid saturation pressure (i.e., temperature) rose with successive TVS cycles while the tank pressure was kept within the control band. When the control mode was changed to maintaining liquid saturation pressure within a prescribed band, the tank pressure then dropped in a saw-tooth fashion with successive cycles.

The only previous TVS test at the NASA Glenn Research Center was an LN_2 test using an axial jet mixer and a multiple-orifice J–T device in a 1.4-m^3 flightweight tank (Ref. 6). Results were obtained at three fill levels at a tank pressure of approximately 145 kPa, and no GHe pressurant was used. The axial jet mixer is a simpler alternative to the spray bar concept tested at Marshall. Extensive testing of the mixing capabilities of the axial jet has been conducted in normal gravity, in drop towers, and on orbit (Refs. 7 and 8). The multiple-orifice J–T device has been proposed as an alternative to a valve. The device has a number of larger diameter spin chambers that may reduce the possibility of clogging due to contaminants, and it has no moving parts. Multiple-orifice J–T devices have been tested in LH_2, LN_2, and LCH_4 (Refs. 9 to 11).

1.2 Modeling and Theory

A simple spreadsheet tool was developed to characterize TVS behavior for a propellant pressurized with GHe given a few input parameters and assumptions. Fluid properties were obtained using software subroutines (Ref. 12) linked to the spreadsheet. The model predicts the thermodynamic state of the propellant tank at the times in the overall TVS cycle when the pressure and temperature are at local minimums. These times occur at the end of each successive TVS cycle at the moment when the pump is switched off and the TVS vent is closed. Assumptions at these points in time follow:

(1) The entire tank contents are isothermal (well mixed).
(2) The binary ullage mixture consisting of propellant vapor and gaseous helium has a uniform mole fraction throughout.
(3) The partial pressure of the vapor is equal to its saturation pressure at the existing temperature.
(4) The partial pressure of GHe equals the tank pressure minus the partial pressure of the vapor.

Parameters input to the model were propellant type (i.e., O_2, CH_4, H_2, or N_2), tank volume, initial liquid fill fraction, energy input to the tank over a complete TVS cycle (environmental heat leak plus dissipated pump power), and the initial temperature and/or pressure. There are three modeling cases:

Case 1—Constant Temperature: The model determines the final pressure.

Case 2—Constant Pressure: The model determines the final temperature.

Case 3—Constant Temperature and Pressure: The model determines the mass of added GHe.

The model is based on three conservation laws: mass conservation of propellant (liquid and vapor), mass conservation of GHe, and an energy balance applied to the tank contents plus propellant vented by the TVS. For Case 2, the energy balance could include the change in tank wall energy (because temperature is not constant); however, the change in wall energy was found to be negligible for all the examples considered. For Case 3, the energy balance included the energy of the added helium.

Thermodynamic properties of the fluid components were calculated as follows (all symbols used in this document are also defined in the Appendix):

(1) The tank volume V_t and fill fraction F were used to determine the liquid and ullage volumes (V_ℓ and V_u).

$$V_\ell = FV_t \tag{1}$$

$$V_u = (1 - F)V_t \tag{2}$$

(2) The temperature T was used to determine the vapor's partial pressure P_v.

$$P_v = P_{\text{sat}}(id, T) \tag{3}$$

where subscript "sat" refers to saturated and "*id*" is the propellant identification.

(3) The partial pressure of helium P_{He} was calculated.

$$P_{\text{He}} = P - P_v \tag{4}$$

where P is the pressure of the tank.

(4) The densities ρ were obtained from a fluid properties program using the proper temperatures and pressures.

$$\rho_\ell = \rho_\ell(id, P, T) \tag{5}$$

$$\rho_v = \rho_g(id, T) \tag{6}$$

$$\rho_{\text{He}} = \rho_{\text{He}}(P_{\text{He}}, T) \tag{7}$$

where the subscripts ℓ, v, and g refer to "liquid," "vapor," and "saturated vapor."

(5) The masses m of each fluid component were calculated.

$$m_\ell = \rho_\ell V_\ell \tag{8}$$

$$m_v = \rho_v V_u \tag{9}$$

$$m_{\text{He}} = \rho_{\text{He}} V_u \tag{10}$$

(6) The internal energy U of each fluid component was the product of the component's mass and specific internal energy u obtained from the fluid properties program.

$$U_\ell = m_\ell u_\ell(id, P, T) \tag{11}$$

$$U_v = m_v u_g(id, T) \tag{12}$$

$$U_{\text{He}} = m_{\text{He}} u_{\text{He}}(T, P_{\text{He}}) \tag{13}$$

(7) The total internal energy of the tank was the sum of the components:

$$U = U_\ell + U_v + U_{\text{He}} \tag{14}$$

The conservation laws were applied to two consecutive TVS cycle minimums denoted as states 1 and 2. For the first calculation, state 1 was the initial condition. For the following cycles, the previous state 2 became the new state 1.

The procedure for Case 2, pressure-controlled operation ($P_2 = P_1$) follows:

(1) Determine all the properties given by Equations (1) to (14) for state 1.

(2) Specify the energy Q added to the system between states 1 and 2.

$$Q_{1\to 2} = \left(\dot{Q}_e + \lambda_p \dot{Q}_p\right) t_{\text{cycle}} \tag{15}$$

where $\dot{Q}_e$ and $\dot{Q}_p$ are the environment heat leak rate into the tank and the rate of pump power dissipation into the tank fluid, λ_p is the pump duty cycle (fraction of time that the pump is turned on), and t_{cycle} is the elapsed time for a single TVS cycle.

(3) Guess the temperature at state 2, T_2.

(4) Determine the propellant and GHe partial pressures at state 2.

(5) Determine the densities of liquid, vapor, and GHe at state 2.

(6) Use the conservation of helium mass relation ($m_{\text{He},1} = m_{\text{He},2}$) to find the fill fraction at state 2:

$$F_2 = 1 - \frac{m_{\text{He},2}}{\rho_{\text{He},2} V_t} \tag{16}$$

(7) Use the fill fraction to determine liquid and ullage volumes at state 2.

(8) Calculate the mass of the liquid, vapor, and GHe using the densities and volumes for each at state 2.

(9) Use the conservation of mass relation for the propellant to determine how much propellant has been vented (denoted by subscript o) between states 1 and 2.

$$m_o^{\ddagger} = m_{\ell,1} + m_{v,1} - \left(m_{\ell,2} + m_{v,2}\right) \tag{17}$$

where ‡ indicates that the value was derived from mass balance.

(10) Calculate the internal energy of the liquid, vapor, and GHe at state 2.

(11) Determine the enthalpy of the vent flow leaving the tank, h_o. For this work, the vent exit temperature was assumed to equal the temperature in the tank and the vapor was assumed to be saturated at the vent exit temperature. Furthermore, the vent flow enthalpy was assumed to be constant from state 1 to state 2. (For Case 2, T_2 was used to obtain h_o.)

(12) Use the conservation of energy relation to determine how much propellant has been vented between states 1 and 2.

$$m_o^{\lozenge} = \frac{U_1 - U_2 + Q_{1\to 2}}{h_o} \tag{18}$$

where the superscript ◊ indicates derived from energy balance.

(13) Use the spreadsheet's goal-seeking tool to find the value of T_2 that makes the results of Equations (17) and (18) identical:

$$m_o^{\ddagger} - m_o^{\lozenge} = 0 \tag{19}$$

(14) The spreadsheet now contains the correct values for vented mass between states 1 and 2, and the fill level and temperature for state 2.

(15) Repeat for as many TVS cycles as desired by making the new state 1 equal to the old state 2.

The procedure for Case 1, temperature-controlled TVS, is similar to that for Case 2 (just presented) except that the final temperature is specified (equal to the initial temperature) and the equations are solved for the final pressure. The procedure for Case 3, temperature and pressure-controlled TVS, is also similar, except that both the final temperature and pressure are equal to the initial values and that the unknown variable (requiring an initial guess) is the GHe mass added from state 1 to state 2, m_i. Therefore, in Step 6, $m_{\mathrm{He},2} = m_{\mathrm{He},1} + m_i$. The temperature and pressure at the GHe inlet to the tank are needed to determine the enthalpy of the added GHe, h_i. In this work, 300 K and the tank pressure were used. Equation (18) should be modified to include the enthalpy of the added GHe in the energy balance:

$$m_o^{\lozenge} = \frac{U_1 - U_2 + Q_{1\to 2} + m_i h_i}{h_o} \tag{20}$$

2.0 Comparison of Model Predictions With Previous Test Results

Two reported TVS test results—the Marshall LCH_4 test (Ref. 4) and an earlier test with LH_2 (Ref. 5)—were compared with the model predictions. These tests had a number of similarities as well as significant differences. The key differences emphasized herein are the helium mole fraction and heat input: both were quite large for the CH_4 test and very small in comparison for the hydrogen test. The fill fraction was about 0.9 for both.

Model predictions for two sets of TVS cycles from the CH_4 test were generated. The required values input to the model were obtained from Reference 4 or estimated by hand digitizing the temperature and pressure plots from the figures in Reference 4. The first set of cycles was modeled as six pressure-controlled cycles (cycle minimums labeled 1 to 7 in Fig. 2 in Ref. 4). The second set of cycles was modeled as six temperature-controlled cycles (cycle minimums labeled 11 to 17 in Fig. 3 in Ref. 4). The pump power was assumed to be 50 W for the CH_4 tests. (Because of the high reported heat leak (720 W) and the low pump-duty cycle, the predicted results were not highly sensitive to the pump power unless the pump power was much greater than the assumed value.)

In Figure 3, the line is an approximate representation of the observed LCH_4 temperature rise during a portion of the test that was under pressure-controlled TVS operation. The symbols indicate the predicted minimum temperatures at the end of each TVS cycle. The model underpredicted the experimental rate of temperature rise by about 40 percent. The GHe mole fraction was approximately 0.65, and the dimensionless heat input (discussed in Sec. 3.0) was about 1.8.

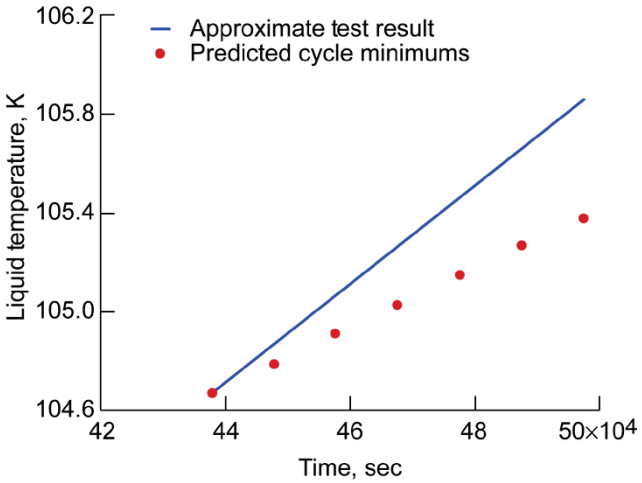

Figure 3.—Comparison of model prediction with NASA Marshall Flight Center liquid methane test results for pressure-controlled thermodynamic vent system (TVS) operation (approximate test result data from Ref. 4).

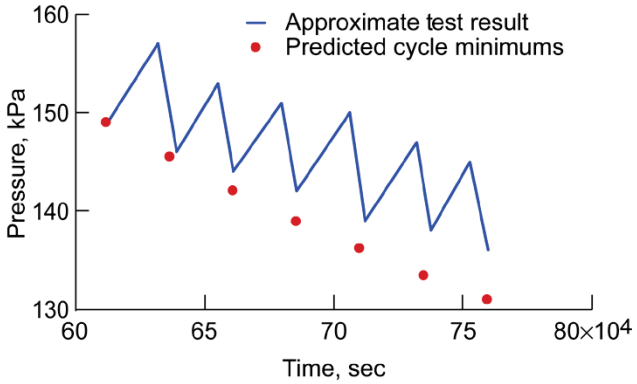

Figure 4.—Comparison of model prediction with Marshall liquid methane test results for temperature-controlled thermodynamic vent system (TVS) operation.

Figure 4 shows an approximation of the tank pressure cycles (only the minimum and maximums were digitized) for a part of the LCH_4 test with temperature-controlled TVS operation as well as the cycle minimum points predicted by the model. The model overpredicted the experimental rate of pressure drop by about 40 percent. For the temperature-controlled test segment shown, the GHe mole fraction was approximately 0.55 and the dimensionless heat input was about 4.4.

Considering the simplicity of the model and the uncertainty in some of the input values, the model did a reasonably good job of matching the experimental trends: the key point is that pressure-controlled operation caused an increase in liquid temperature, whereas temperature-controlled operation caused the tank pressure to drop.

This TVS behavior (pressure drop or temperature rise) observed during the Marshall methane test had not been observed in previous TVS tests. A test from Reference 5 for LH_2 pressurized with GHe at 90-percent fill was selected for comparison with the model. In the selected LH_2 case, the helium mole fraction was 0.037. After a long transient period involving mixing without venting and heating the liquid, about 20 consecutive TVS cycles were conducted using pressure-control logic. The tank pressure cycled within the lower and upper control points. The liquid temperature appears to be steady in Figure 6 in Reference 5. The model for this test predicted a temperature rise over the 20 cycles of 0.01 K—a very minor increase that would be difficult to detect. The model assumed a pump power of 25 W, which—combined with the reported values of tank volume, environmental heating rate, duty cycle, and cycle time—resulted in a relatively low dimensionless (*) heat input value of $Q^* = 0.41$. Therefore, the helium mole fraction and the heat input in this test appear to have been sufficiently low to result in the unnoticeable temperature rise during pressure-controlled operation.

Another finding from modeling the Marshall LH_2 TVS test was that there was substantial loss of GHe from the ullage because of solubility in the liquid. In the test, the amount of GHe added to the ullage was metered. The amount was 0.34 kg. However, on the basis of the test pressure, temperature data, and modeling assumptions, the GHe in the ullage should have been 0.25 kg. If both values are correct, then 0.09 kg of GHe must have dissolved in the liquid. Given sufficient spray-bar operating time, the calculated amount of dissolved GHe is possible because of the vigorous liquid-ullage interaction resulting from liquid droplets passing through the ullage during spray-bar operation. The maximum amount of GHe that can be dissolved can be predicted using the correlation for GHe and hydrogen given in Reference 13. At the test pressure of 0.166 MPa and liquid temperature of 21.9 K, the correlation predicts a mole fraction of GHe dissolved into the liquid of 0.00013, which converts to 0.29±0.02 kg of GHe dissolved into the liquid. Therefore, 0.09 kg of GHe lost to solubility is feasible. Loss of GHe from the ullage due to solubility in the liquid is very likely in other TVSs as well, such as the Marshall CH_4 test and the present work.

3.0 Correlation of Model Predictions

Although the model is quite simple, the manner in which the various input values affect the behavior of the TVS cycles is not readily apparent. Therefore, two correlations were developed to capture the major trends predicted by the model. First, the model was used to predict pressure loss per TVS cycle for a range of GHe mole fractions, tank heat values, and tank fill levels for liquid oxygen (LO_2), LCH_4, and LH_2 when the TVS was operated in the temperature-control mode. The results were then correlated to show the significance of these factors. The following dimensionless groups were used:

$$\text{GHe mole fraction: } x_{\text{He}} = P_{\text{He}} / P \tag{21}$$

$$\text{Dimensionless heat input: } Q^* = \frac{\dot{Q}\, t_{\text{cycle}}}{\rho_\ell V_t h_{fg}} \times 1000 \tag{22}$$

where $\dot{Q} = \dot{Q}_e + \beta_{\text{TVS}} \dot{Q}_p$, t_{cycle} is the time for one cycle, and h_{fg} is the latent heat of vaporization.

Liquid fill fraction: F

Dimensionless pressure drop per TVS cycle (in percent):

$$P^* = \frac{P_{int} - P_{fin}}{P_{int}} \times 100 \tag{23}$$

where *int* indicates "initial" and *fin* indicates "final."

$$\text{Dimensionless temperature: } T^{\dagger} = \frac{T - T_{tp}}{T_{cp} - T_{tp}} \tag{24}$$

where the subscripts *cp* and *tp* indicate the critical point and triple point and † indicates the dimensionless quantity in correlation.

The model was run for F from 0.03 to 0.95, using 10 values of F for $T^{\dagger}$ = 0.2, 0.4, and 0.6 for each propellant. Values for x_{He} and Q^* were randomly generated within the ranges $0.01 < x_{He} < 0.7$ and $0.1 < Q^* < 6$ for each pair of (F, $T^{\dagger}$). The ranges of mole fraction, heat input, and temperature covered the experimental values for the current LO_2 test as well as the Marshall LH_2 and LCH_4 tests. Values for x_{He} and F are for the start of a TVS cycle. The correlated predictions are shown in Figure 5 in the form of the following power law fit:

$$P^* = \frac{0.1\, x_{He}\, Q^*}{1 - F} \tag{25}$$

The correlation is quite good. Several trends are evident. First, the pressure drop per cycle is proportional to both the GHe mole fraction and the dimensionless heat input. Second, the pressure drop per cycle is larger at high fill levels (small ullage volume). Third, the correlation is independent of the dimensionless group $T^{\dagger}$. Equation (25) is not reliable for values of $T^{\dagger}$, x_{He}, and F above the upper limits stated earlier in this section.

A second similar correlation of model predictions was developed for the pressure-controlled mode. The dimensionless group P^* was replaced with T^*, which was defined as the dimensionless temperature rise per TVS cycle (in percent):

$$T^* = \frac{T_{fin} - T_{int}}{T_{int}} \times 100 \tag{26}$$

The same ranges of F, $T^{\dagger}$, x_{He}, and Q^* were used. The resulting correlation for T^* was

$$T^* = \frac{0.02\, x_{He}\, Q^*}{(1 - F)^{0.7}} \tag{27}$$

Note that Equation (27) is also independent of the dimensionless group $T^{\dagger}$. The T^* correlation, as shown in Figure 6, is not nearly as tight of a fit as the P^* correlation, but otherwise it exhibits similar trends. That is, the temperature rise per cycle is proportional to the GHe mole fraction and the dimensionless heat input. Also, the dimensionless temperature rise per cycle increases with fill level, but it is a lesser function of fill level than is the dimensionless pressure drop per cycle.

The key point of the correlation development was not so much to obtain the correlations, but rather to better understand

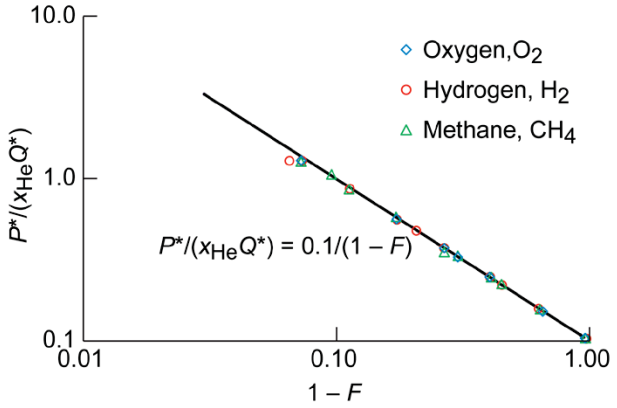

Figure 5.—Correlated model predictions for dimensionless pressure drop per thermodynamic vent system (TVS) cycle; P^*, dimensionless pressure, x_{He}, mass fraction of helium, Q^*, dimensionless heat transfer, and F, liquid fill fraction.

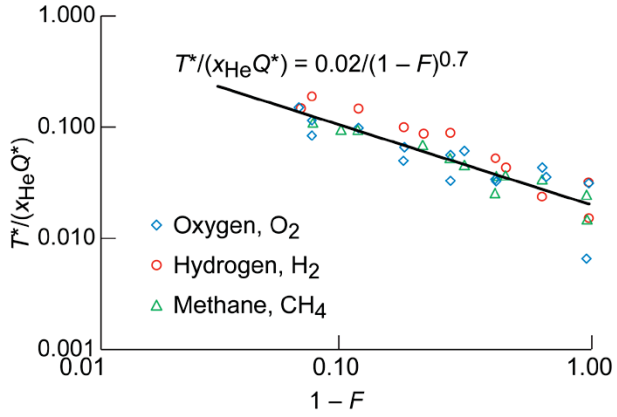

Figure 6.—Correlated model predictions for dimensionless temperature rise per thermodynamic vent system (TVS) cycle; T^*, dimensionless temperature, x_{He}, mass fraction of helium, Q^*, dimensionless heat transfer, and F, liquid fill fraction.

the TVS cycle behavior's dependence on GHe mole fraction and heat input. The correlations show that pressure drop (in temperature-control mode) and temperature rise (in pressure-control mode) were both directly proportional to both GHe mole fraction and heat input.

4.0 Test Overview

The test results presented herein are from the first TVS demonstration using LO_2 conducted by NASA. For most tests, the liquid was heated about 21 K above its normal boiling point and pressurized with helium to about 1.6 MPa. These conditions were chosen to represent (as closely as possible given test facility limitations) operating conditions for a lunar lander ascent-stage oxidizer tank. The resulting GHe mole

fraction (~60 mol%) was comparable to that of the Marshall TVS test with subcooled LCH_4. A benefit of having an elevated liquid temperature relative to the normal boiling point was that the TVS could be vented to the atmosphere with the J–T expansion providing a sufficient temperature drop in the vent flow for successful TVS heat exchanger performance.

Three different fluid mixing configurations were tested: (1) a submerged axial jet with vertical upflow, (2) liquid droplets sprayed directly into the ullage using a pair of spray hoops near the top of the tank, and (3) combined flow using the axial jet and spray hoops simultaneously. Figures 7 and 8 show simple diagrams of the axial jet and spray hoop concepts, respectively. Optimization of the pump operation duration prior to venting was not possible because of time constraints. The time delay between pump startup and vent valve opening did not appear to be beneficial in the tests with GHe pressurization, so the delay time was reduced for these tests.

Two special tests also were conducted: one without GHe pressurization and another with LN_2 as the test liquid. The test without GHe was primarily an initial checkout to verify TVS operation and to test automated control using two modes of control logic. For this test only, the pump was briefly operated prior to venting in each TVS cycle to destratify the liquid. The LN_2 test allowed further testing with a second test fluid and was also used to demonstrate more advanced control logic using systematic helium repressurization. All of the special tests were performed with the axial jet configuration. Boiloff testing was done to quantify the environmental heating rate of the test. Table I summarizes the conditions for each test series performed: Test Series A through E.

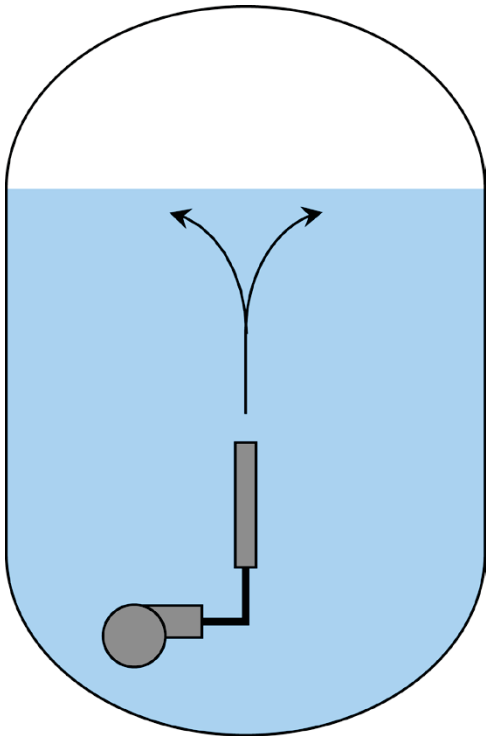

Figure 7.—Axial jet.

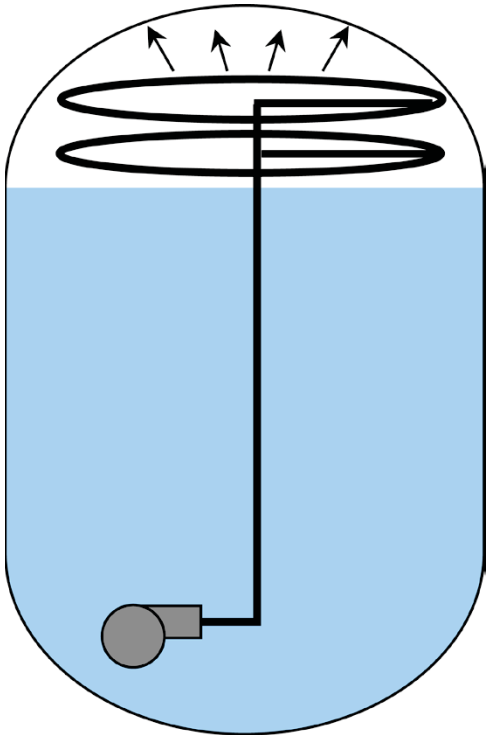

Figure 8.—Spray hoops.

TABLE I.—SUMMARY OF COMPLETED TESTS AND CONDITIONS[a]

Test series	Hardware configuration	Test fluid[b]	Approximate test pressure, MPa	Boiloff test at ~95-percent fill	TVS[c] test at ~90-percent fill	TVS[c] test at ~50-percent fill	Boiloff test at 40-percent fill
A	Axial jet	O_2 only	0.6	Yes	Yes	Yes	No
B	Axial jet	O_2/GHe	1.5 to 1.6	No	↓	↓	Yes
C	Axial jet and spray hoops	O_2/GHe	1.3 to 1.6	No			No
D	Spray hoops	O_2/GHe	1.4 to 1.6	Yes			No
E	Axial jet	N_2/GHe	1.6	No	No		No

[a]Pressures and fill levels are approximate. See test result sections for detailed information.

[b]O_2, oxygen; GHe, gaseous helium; N_2, nitrogen.

[c]TVS, thermodynamic vent system.

5.0 Test Apparatus and Instrumentation

The test tank was cylindrical with domed ends plus a smaller upper cylindrical section with a domed lid. It had a main diameter of 1.22 m and an overall height of 1.91 m. The upper section had a diameter of 0.48 m and a height of 0.34 m. The tank was made of stainless steel and had a wall thickness of 0.95 cm. Total tank volume was approximately 1.64 m^3. The tank and tank lid were bolted together at matching flanges at a location corresponding to a fill level of approximately 98 percent. The lid had seven ports for plumbing and electrical feedthroughs. Four additional ports were located at the tank bottom. Figure 9 shows the bare test tank prior to installation of the multilayer insulation (MLI). The tank is shown suspended from the vacuum chamber lid, which is supported by the blue framework.

Eighteen thermocouples were attached to the exterior surface of the test tank at various locations to monitor the tank wall and lid temperatures. A 432-W band heater was clamped around the tank at the 27-percent fill level. The heater was used only to heat the liquid in the tank to the desired test temperature. The tank was insulated with three layers of MLI. The inner and outer layers were made of an aluminized tear-resistant material, and the center layer was double-aluminized polyethylene terephthalate (PET) film. The layers were separated by polyester netting. Figure 10 is a photograph of the test tank after installation of the MLI. The purpose of the MLI was not so much to reduce heat leak: it was necessary to allow the test tank to absorb heat quickly so that a suitable number of TVS cycles could be performed in a relatively short time. Instead, a minimal number of MLI layers were used to provide at least some resemblance to flight hardware.

The test tank was suspended from three load cells used to weigh the tank to measure liquid fill levels accurately. Each load cell had a full-scale range of 8900 N and a static error band (accuracy) of ±0.03-percent of full scale. The load cells were designed as calibration reference standards. A calibration system was used to calibrate the tank-weighing system, which is shown with its calibration hardware in Figure 11. The calibration system consisted of a rigid beam that could rotate about its midpoint position in a bearing assembly anchored to the floor underneath the vacuum chamber. The end of the beam directly below the center of the vacuum chamber could exert a downward force on the test tank via a linkage that passed through a port with a flexible bellows in the bottom of

Figure 9.—Test tank prior to installation of multilayer insulation.

Figure 10.—Test tank with multilayer insulation installed.

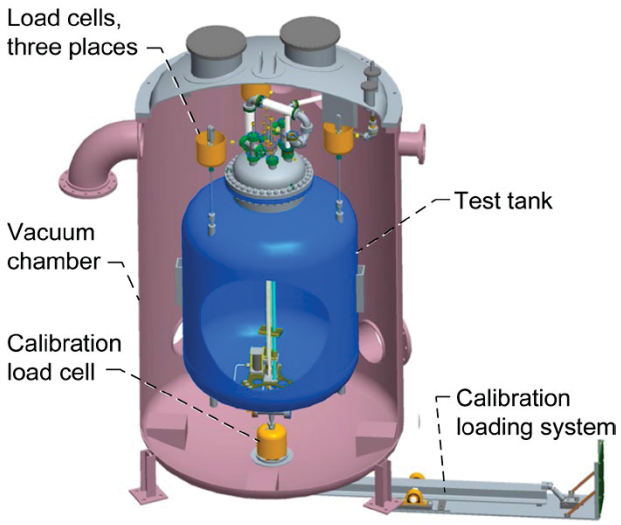

Figure 11.—Weighing system and calibration hardware.

the vacuum chamber. The linkage included a calibration load cell. The bellows design eliminated any sensitivity of the calibration load on the external-to-internal pressure difference, and the linkage was decoupled during actual testing. The opposite end of the rigid beam was loaded with an upward applied force from a hand-activated pneumatic jack. Therefore, the applied load acted on the weighing system and could be directly measured with the calibration load cell.

The tank vent and fill lines were constructed with multiple flex hose sections to minimize additional load forces acting on the test tank. Other physical connections between the vacuum chamber lid and the test tank, such as the fluid-sampling tubes, tank pressurization line, and electrical leads, had greater compliance and minor impact on the weighing of the tank. The fill and vent lines had a small impact on weighing system performance because the flex lines stiffened and moved when pressurized. This effect was accounted for in the calibration of the weighing system. The calibration equation for the fluid mass (liquid plus vapor) follows:

$$m_{fl} = \alpha \sum_{j=1}^{3} R_{lc_j} + \beta P + \gamma \tag{28}$$

where the first term on the right is the sum of the three individual load cell readings R_{lc_j}. The second term is a small correction for the effects of tank pressure and the third term is approximately equal to the tare weight of the test tank. For the series of tests reported herein, the values for the coefficients were

$$\alpha = 0.10222 \text{ kg/N} \quad \beta = -4.1076 \text{ kg/MPa} \quad \gamma = -773.66 \text{ kg} \tag{29}$$

The calibration fitted 330 data points of simulated fluid weight to within 0.25 percent of the tank full-scale weight (LO_2 at 111 K and 1.59 MPa), and the calibration error band accounts for the repeatability, hysteresis, and nonlinearity of the system. The weighing system was used primarily to determine liquid fill level, but because it could sense small changes in level, it was useful as a secondary method of measuring outflow rates during boiloff or TVS testing.

A submersible, centrifugal liquid oxygen pump that was designed for 37.9 liters/min at 2920 rpm with a 6.1-m head was located inside and near the bottom of the test tank. The direct-current (DC) pump motor power was 100 W at the maximum speed of 3500 rpm (120 percent of the design speed). The pump was operated at the design speed for all tests. It could also be operated in LN_2, but at an off-design head condition.

The TVS heat exchanger was attached at the pump inlet as shown in Figure 12. The heat exchanger is a coiled-loop design where the TVS vent flow flowed through 22 loops of tubing located between cylindrical inner and outer shells. On the hot side of the heat exchanger, liquid flowed through the annulus over the external surface of the coiled tube and then into the pump inlet. Further details about the modeling and design of the heat exchanger are available elsewhere (Ref. 14). The discharge from the pump was flowed through piping to hand valves mounted outside the tank where the flow could be routed to either a submerged axial jet or a pair of spray hoops near the top of the tank via separate lines to each that reentered the tank. Flow for the cold side of the heat exchanger was drawn from a well formed by one of the bottom tank ports and was routed through a Visco Jet (Lee Company, Westbrook, CT) (Ref. 15) with a flow resistance rating of 5000 Lohm.[1] The Visco Jet was a multiple-orifice flow restrictor used as a J–T expansion device. After expanding to a lower pressure and temperature, the cold-side vent flow was vaporized as it flowed through the coiled loops of the heat exchanger and then routed out of the tank bottom and through the vacuum chamber lid to an atmospheric vent system containing vent gas flowmeters (discussed later in this section). Figure 13 shows the internal hardware and instrumentation suspended from the test tank lid, and Figure 14 shows the internal hardware and instrumentation installed in the bottom of the test tank. Figure 15 is a photograph of the TVS plumbing on the outside of the test tank.

In a previous TVS experiment at Glenn (Ref. 6), it was observed that the submerged portion of the TVS vent line would fill with liquid under no-flow conditions. Each time venting was initiated, a liquid slug would pass through the vent line without effective vaporization. The corresponding loss of cooling resulted in reduced TVS efficiency. For the present series of tests, a cryogenic coaxial solenoid (shutoff)

[1]A measure of fluid resistance (http://www.theleeco.com/engineering/lohm-definition.cfm Accessed Feb. 2014).

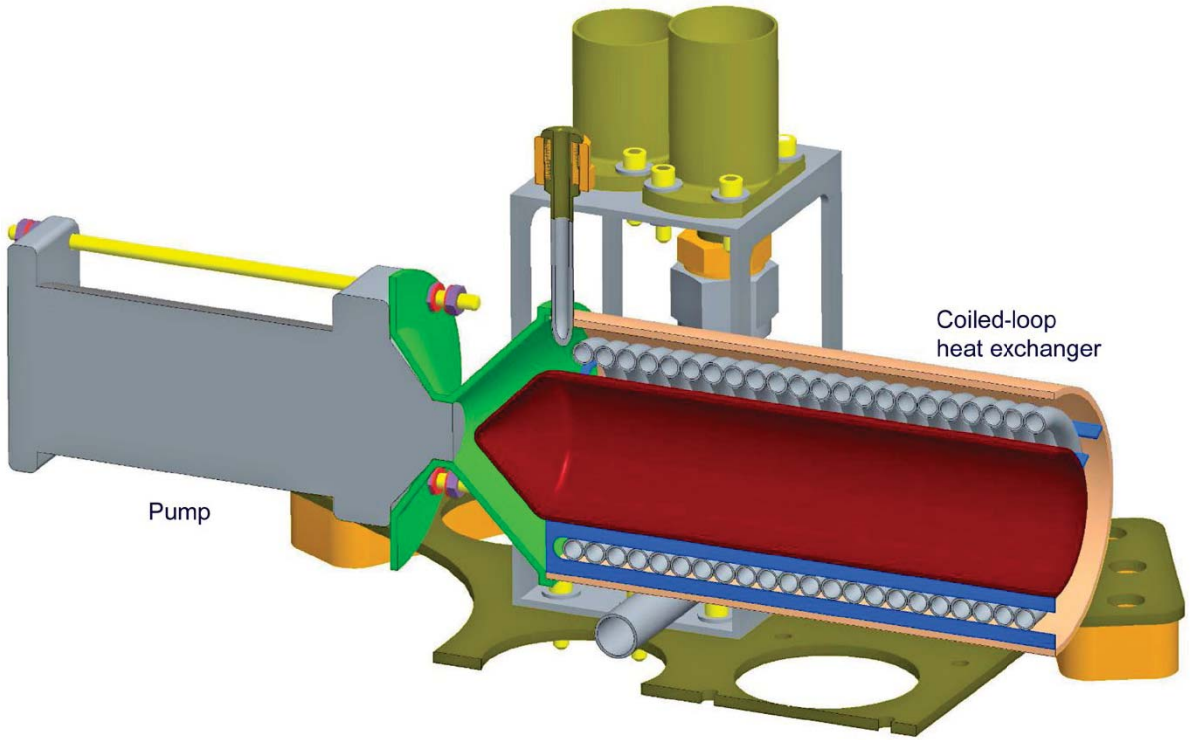

Figure 12.—Thermodynamic vent system (TVS) heat exchanger and pump assembly.

valve was installed in the inlet line upstream of the J–T device. This valve could not be placed inside the tank, however, so the inlet flow was routed out of a bottom port, through the solenoid valve, and back into the tank to the J–T device. The solenoid valve generated heat when energized, and because it was operated in a vacuum environment, an aluminum thermal strap was fabricated to transfer heat to the vent line outside the test tank. As an additional precaution, the thermal strap was cooled with LN_2 from an external source.

The axial jet was constructed of stainless steel tubing with an inner diameter of 1.65 cm. The discharge orifice in the axial jet's end cap had a diameter of 1.02 cm and was located at a height corresponding to the 34-percent fill level. The axial jet was offset from the tank's vertical axis by approximately 0.2 m as shown in Figure 14. The upper and lower spray hoops were both constructed of 1.27-cm-diameter stainless steel tubing. Both hoop diameters were 0.43 m, and the hoops were centered about the tank's vertical axis along with the tank fill/drain tube. The upper hoop had 36 discharge holes directed upward or upward/inward. The lower hoop had 102 discharge holes angled either upward/outward, upward/inward, or slightly downward/inward. All spray hoop discharge holes had diameters of 1.5 mm. The vertical supply pipe from the pump to the hoops had a 1.9-cm diameter. The upper spray hoop was located at a height corresponding to the 99-percent fill level, and the lower hoop was located at a height corresponding to the 94-percent fill level.

Instrumentation inside the test tank included two vertical temperature sensor rakes mounted near the tank's central axis. Rake A contained 11 silicon-diode temperature sensors positioned at 5-, 10-, 20-, 30-, 40-, 50-, 60-, 70-, 80-, 90-, and 95-percent fill level locations. Rake B contained 10 silicon-diode sensors at the 15-, 25-, 35-, 45-, 65-, 75-, 85-, 96-, 97-, and 99-percent fill level locations plus two close-spaced diode clusters with sensors located at 1-percent intervals from 46- to 55-percent fill and 86- to 95-percent fill. One purpose of the diode clusters was to measure temperature gradients near the liquid surface at the two nominal fill levels of 50 and 90 percent. The second function of the diode clusters was to sense liquid level by operating the diodes in a high current mode to determine which sensors were submerged and which ones were exposed to the ullage. Only the diodes in the two clusters were set up to sense liquid level. Other silicon diode temperature sensors were located inside the piping to measure the temperature at the entrance to the upper and lower spray hoops, near the axial jet, at the pump discharge, upstream and downstream of the J–T device, and in the flow downstream of the heat exchanger on the vent side (two sensors).

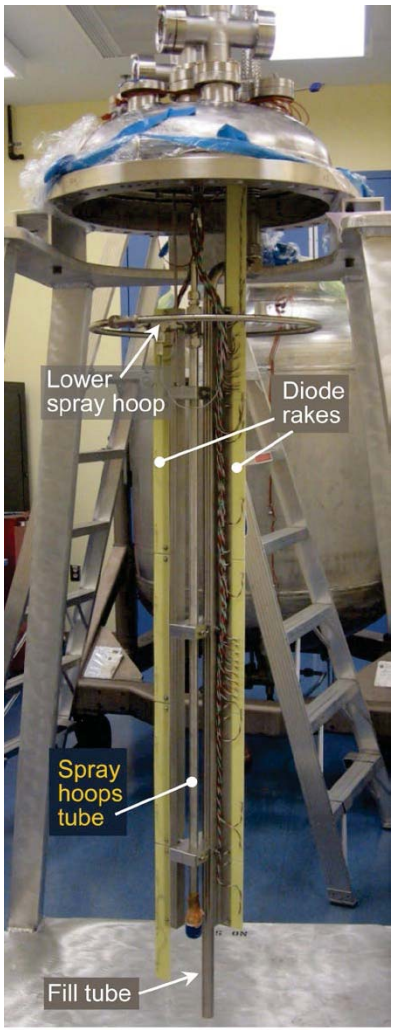

Figure 13.—Internal hardware and instrumentation suspended from the test tank lid. (The upper spray hoop is hidden from view.)

The remaining piece of instrumentation inside the tank was a venturi meter located downstream of the pump and upstream of the flow control valves to the axial jet and spray hoops. The only significant instrumentation failure during the test was a cryogenic differential-pressure sensor attached to the venturi meter. Two sensing lines were routed out of the test tank bottom with short tubing extensions to connect to the differential-pressure sensor. These lines and the transducer body, but not the electronics module, were insulated with MLI insulation. The output from the differential-pressure sensor was not consistent, and the zero-flow reading had substantial shifts from day to day. The venturi meter results were deemed to be unreliable and are not reported.

Outside of the test tank, there were three internal flow-sensing thermocouples located along both the fill and vent lines to measure fluid temperatures. Each of these lines also had two additional thermocouples attached to the external walls. The TVS vent line had a wall-attached thermocouple on each side of the thermal strap attachment point plus another near the vacuum chamber lid. Pressure inside the test tank was sensed by a pressure sensor attached to the ullage vent line. Other external data recorded included the test facility indoor temperature, outdoor temperature, and barometric pressure.

Two digital thermal-type mass flowmeters were installed in the test tank's vent line. A 500-slpm meter was used[2] to measure flowrates during TVS venting. A 20-slpm meter was intended to measure steady-state boiloff rates. The manufacturer's reported accuracy specifications were ±1.0 percent of the full-scale rating (FS) above 20 percent of FS and ±0.2 percent of FS below 20 percent of FS. Furthermore, the meters had a 50:1 turndown ratio (1/50 is 2 percent of FS), below which the readings were unreliable. Both meters were calibrated by Glenn's Calibration Laboratory at the conclusion of the test program. The large meter was calibrated with air, and the small meter with nitrogen gas. The calibration results were fitted with a linear equation having a zero intercept. The calibration factors were 1.019 for the large meter and 1.0026 for the small meter.

The manufacturer's conversion factors were 0.998 for air, 1.000 for nitrogen, and 0.988 for oxygen. Therefore, the conversions used for oxygen flowrates were 0.988/0.998 = 0.990 for the large meter and 0.988 for the small meter. Similarly for nitrogen TVS flowrates, the conversion for the large flowmeter was 1.000/0.998 = 1.002. (The small meter was not used with nitrogen because there was no nitrogen boiloff test.) For the conversion of volumetric flowrate to mass flowrate, the appropriate densities for oxygen or nitrogen had to be used. Density was based on the referenced standard pressure and temperature at calibration. Both meters were calibrated using a standard pressure of 101.3 kPa (1 atm), but the reference temperatures were different: 21.1 °C for the large meter and 0 ºC for the small meter. The corrected measured flowrate was calculated as follows:

$$\dot{m}_o = \rho_{\text{ref}} R_{fm} C_{\text{cal}} C_{\text{fluid}} \tag{30}$$

where C is the flowmeter coefficient and the subscripts ref, *fm*, and cal indicate reference, flowmeter, and flowmeter calibration.

[2]Standard liters per minute.

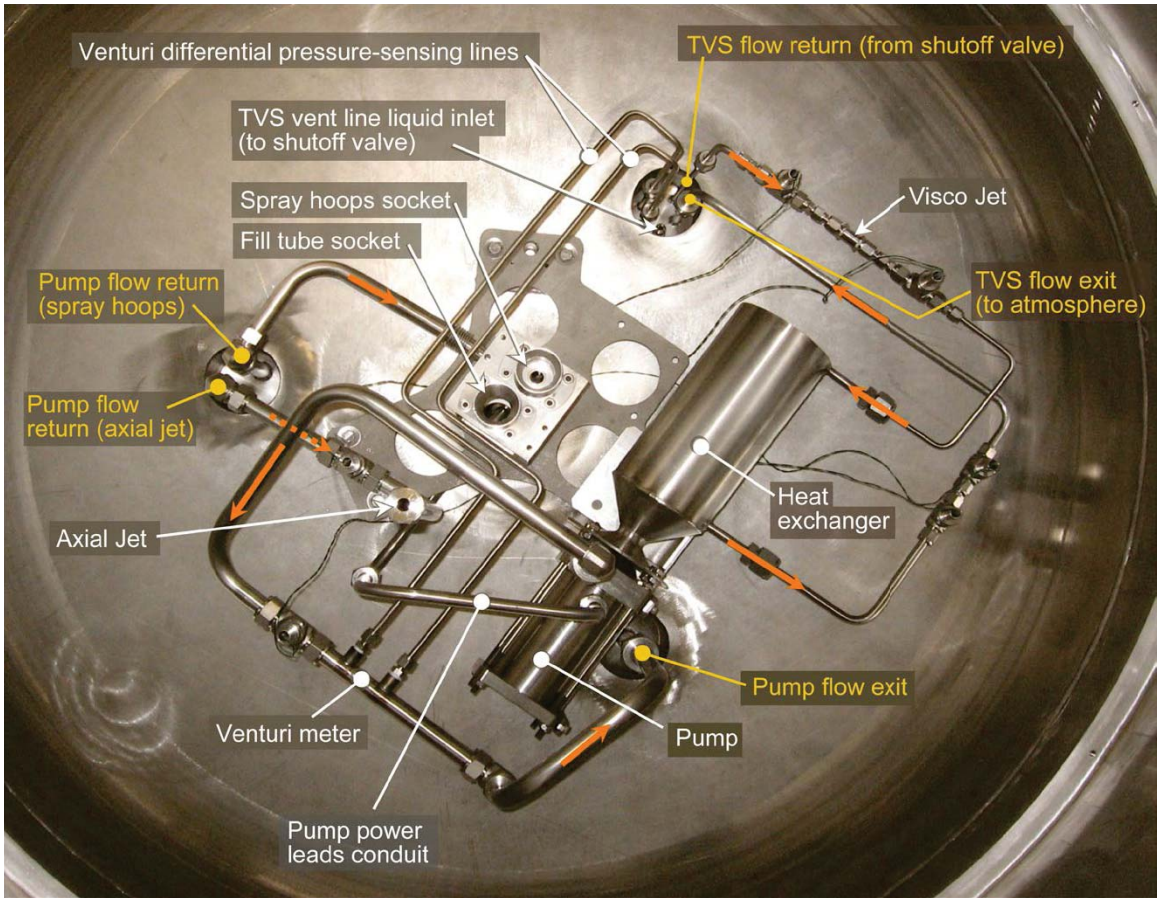

Figure 14.—Internal hardware and instrumentation in the bottom of the test tank; TVS, thermodynamic vent system.

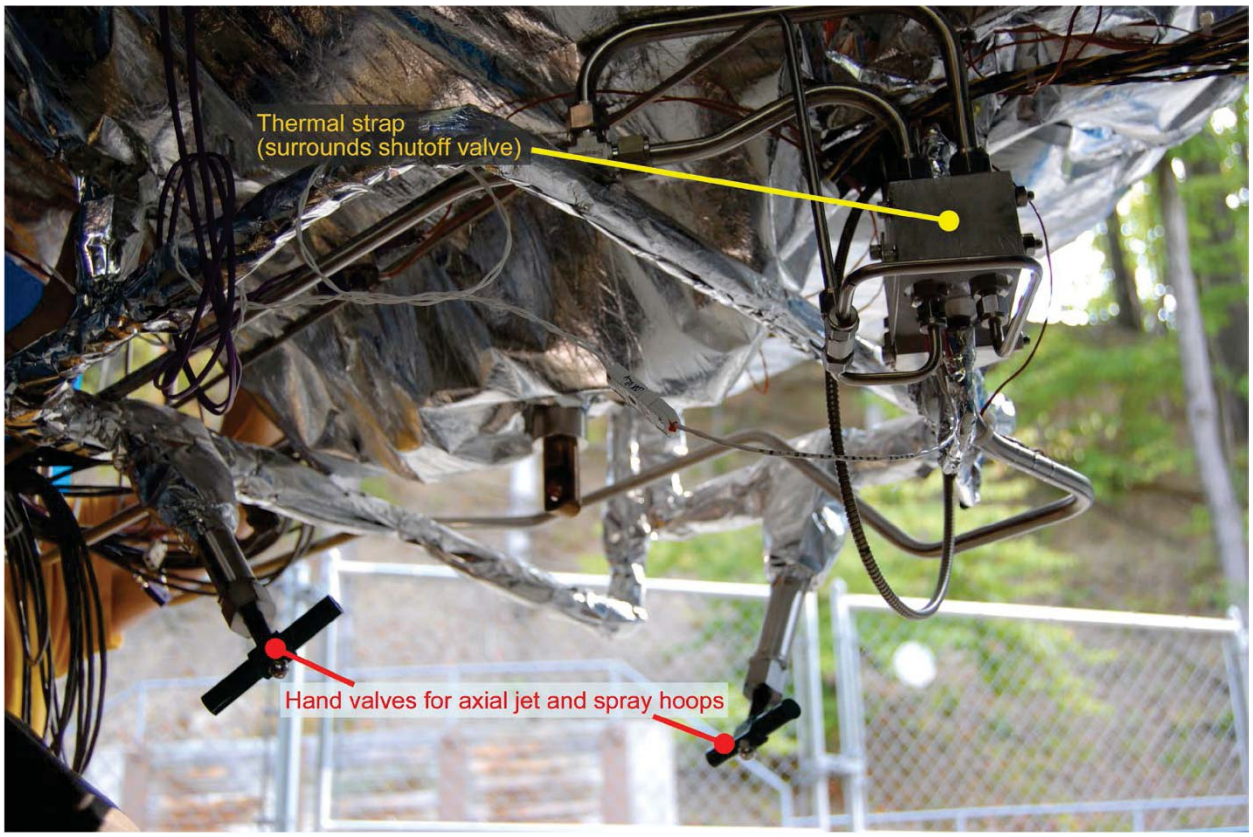

Figure 15.—Thermodynamic vent system (TVS) plumbing outside the test tank.

6.0 Thermodynamic Vent System Control Logic and Interaction With Data System

The control logic developed for the present series of tests allowed automatic and unattended operation of the initial heating and self-pressurization portion of the test as well as TVS operation. Human intervention was only required to start the test, switch TVS control between pressure or temperature control modes, adjust the tank pressure (by adding GHe pressurant), and change the tank fill level. Various input parameters could be changed while a test was in progress, but generally, these parameters were not modified during a particular test other than to switch between pressure and temperature control. The number of desired TVS cycles was generally set to a large number so that the tests would not stop during unattended operation.

Figure 16 shows a flow chart showing the control logic. User input parameters follow:

(1) Lower limit for the tank pressure, P_{min}
(2) Upper limit for the tank pressure, P_{max}
(3) Lower limit for the average liquid temperature, T_{min}
(4) Upper limit for the average liquid temperature, T_{max}
(5) Time delay t_{el0} for checking if the maximum pressure or temperature has been reached
(6) Time delay t_{el1} for checking the rate of tank pressure decay while the pump is operating with the vent valve closed
(7) Time delay t_{el2} for checking if the minimum pressure or temperature has been reached
(8) The value of tank pressure decay rate (DPDT) at which a decision is made whether or not to open the vent valve
(9) Choice of tank pressure control or average liquid temperature control (CntrlFlg)

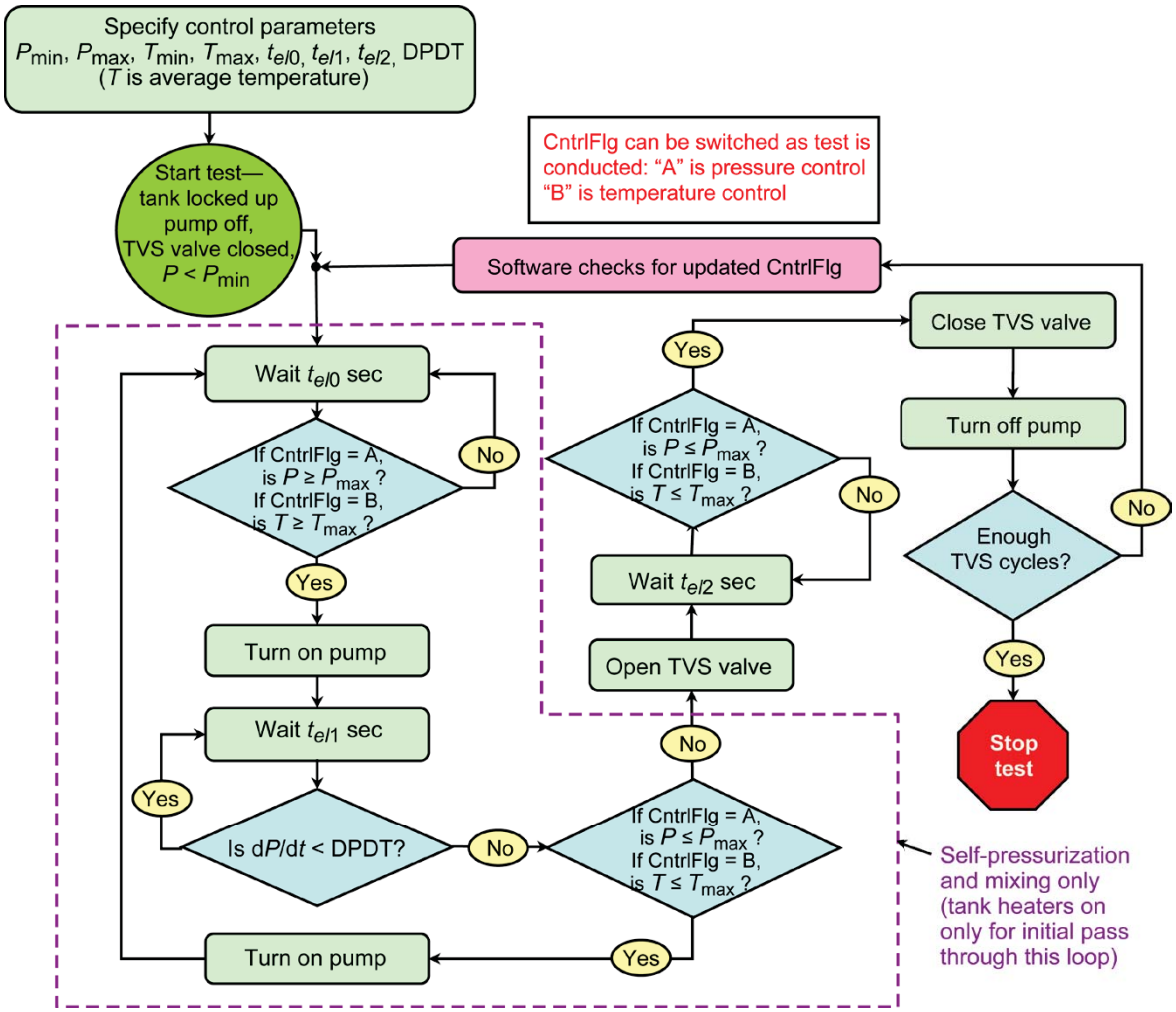

Figure 16.—Flow chart of control logic for heating/self-pressurization and thermodynamic vent system (TVS) operation; P, pressure; t_{el}, elapsed time for type of control logic; CntrlFlg, flag for user-specified temperature- or pressure-control logic; and T, temperature; DPDT, user-specified tank pressure decay rate in control logic.

The control logic was programmed into the test facility control software and required information exchange with the data system. The data system provided real-time values of the tank pressure and the averaged liquid temperature. All of the silicon-diode temperature sensors inside the test tank were available for use in determining the (arithmetic) average temperature. A user interface in the data system allowed convenient selection of the desired sensors. The first attempt to define the average temperature using four or five distributed sensors (all submerged in the liquid) worked well, and this method was kept throughout the test program. For tests at 90-percent fill, the sensors at the 10-, 30-, 60-, and 80-percent fill locations were used; and for tests at 50-percent fill, the sensors at the 10-, 20-, 30-, and 40-percent fill locations were used. Two recording rates were used by the data system: a slower rate when the pump was off (one recording per 90 to 240 s, typically 180) and a faster rate when the pump was operating (one recording per 60 to 180 s, typically 90). The control software would turn the pump off and on and share the pump status with the data system. Noise in the data could cause errors in the decisionmaking steps. Therefore, time delays were inserted in the logic. The data system scanned all data channels approximately twice a second.

7.0 Signal Conditioning

Early in the tests, additional steps were required to improve control performance, leading to signal-conditioning improvements for both rate of pressure change and average liquid temperature. Calculating the rate of change of pressure using consecutive readings could produce a noisy and unstable result, especially when one was looking for dP/dt to approach a constant value (such as 0). A smoothing function was used:

$$\frac{\mathrm{d}P}{\mathrm{d}t} = \zeta \left.\frac{\mathrm{d}P}{\mathrm{d}t}\right|_{\text{new}} + (1-\zeta)\left.\frac{\mathrm{d}P}{\mathrm{d}t}\right|_{\text{old}} \tag{31}$$

where ζ was typically 0.1 to 0.2. The function worked well to smooth the dP/dt signal. The computed value of dP/dt lags the true value, but the lag was not a significant issue for TVS control because of the much longer time scale of the TVS cycles.

The average liquid temperature, although typically based on four sensor readings, was initially rather noisy as in Section 11.0. The noise caused control problems during temperature-control mode when the minimum-to-maximum temperature difference was narrowed (typically 0.17 K). The signal noise was reduced by using a running average of 60 consecutive scans (about 30 s) of data. This averaging interval is short in comparison to the typical TVS cycle time of several hours.

8.0 Boiloff Data Analysis

The environmental heat input rate $\dot{Q}_e$ was determined from the measured boiloff rate as follows:

$$\dot{Q}_e = \dot{m}_o h_{fg}\left(\frac{\rho_f}{\rho_f - \rho_g}\right) + \dot{m}_o\left(h_{ex} - h_g\right) + \frac{V_t}{\phi}\frac{\mathrm{d}P}{\mathrm{d}t} \tag{32}$$

where ϕ is the energy derivative defined in Equation (33) and the subscripts *e* and *ex* indicate "environmental" and "exit," respectively.

The first term on the right-hand side assumes that the tank contains saturated liquid and vapor and that all heat input results in phase change (evaporation). The density ratio accounts for the portion of vapor mass that remains in the tank and occupying the space of the vaporized liquid. The second term on the right-hand side is the heating rate required to heat the vapor exiting the tank from the saturation temperature to the temperature of the superheated vapor at the tank exit (the inlet to the vent line). The tank vent was located at the top of the tank, so the uppermost temperature measurement inside the tank at the 99-percent fill level was used to obtain h_e. The second term is small at very high liquid fill levels, but it becomes significant as the fill level decreases. The last term on the right-hand side is ideally zero when the tank pressure is kept at a constant value during the boiloff test. In the tests reported herein, the pressure drifted slightly and the corresponding change in fluid temperature (resulting in propellant mass gain or loss) should be accounted for. The last term was obtained from a model assuming saturated liquid and vapor (Ref. 16). The energy derivative ϕ is defined as

$$\phi = \frac{1}{\rho}\left(\frac{\partial u}{\partial P}\right)_{\rho} \tag{33}$$

ϕ is calculated numerically (using Ref. 12 to obtain fluid properties) and is dependent on the fill fraction of the test tank as discussed in Reference 16.

The boiloff rate using the weighing system was calculated as

$$\dot{m}_o = \frac{m_{fl,int} - m_{fl,fin}}{t_{fin} - t_{int}} \tag{34}$$

The weighing system calculation was applied to time spans where the fluid mass loss was observed to be linear with time. The accuracy of the boiloff rate calculated from the weighing system depended on the time span used. The estimated accuracy was 4 percent for 10 hr of elapsed time.

9.0 Boiloff Test Results

Three boiloff tests were conducted to quantify the total heat leak rate into the test tank. True steady-state thermal conditions (i.e., steady temperatures, pressures, and boiloff rates) did not consistently occur throughout the TVS tests, and the actual environmental heat input rate was somewhat variable because of differences in the upper tank wall temperatures (e.g., warm unwetted upper wall with axial jet vs. cold-wetted upper wall with spray hoops), small differences in the uncontrolled vacuum chamber wall temperature (no cryoshroud was used) and vacuum level, and variability in the initial thermal conditions prior to the TVS tests. The test schedule also did not allow sufficient time to establish true thermal equilibrium prior to and during each test. As a result, the actual heat input rate during an individual TVS test was not necessarily the same as for other tests or for the boiloff tests. Nonetheless, the boiloff results provide the best available estimate of heat leak rates for the TVS tests.

Table II summarizes the boiloff results. All boiloff tests were conducted with LO_2 and ranged from 34 to 47 hr. Two tests were performed at 93- to 94-percent fill, and one at 39-percent fill. The tank pressure was regulated by automated back-pressure control of the tank's vent system at approximately 0.60 MPa (saturation temperature of 111.5 K). Two independent means of measuring the boiloff rate were used: (1) the boiloff vent flow was routed through gas flowmeters, and (2) the change in fluid mass contained in the test tank was measured by the test tank weighing system.

Unfortunately, the boiloff rate was nearly equal to the full-scale range of the 20-slpm vent line flowmeter, whereas the reading based on the much larger 500-slpm flowmeter was below the lower accuracy limit of the meter's turndown ratio. The smaller meter was over-ranged in Test A. In general, the flowmeter output did not achieve clearly observable steady-state conditions, but it did appear to be approaching reasonably steady behavior. The flowmeter readings and corresponding tank pressure data used for the boiloff analysis are shown in Figure 17.

The two heat leak measurements from the flowmeter (Tests B and D) and the three measurements from the weighing system (Tests A, B, and D) were averaged to obtain a representative total heat leak rate. The heat leak rate was slightly higher for the lower fill-level test, but this trend with fill level was not considered to be meaningful. In the remainder of this report, a heat input rate of 97 W is used. The uncertainty in the heat input rate result was attributed mainly to the insufficient time to reach truly steady conditions and was conservatively estimated to be no greater than ±10 W (10 percent).

In the two high-fill-level tests, the ullage heating component was about 8 to 9 percent of the total. At the lower fill level, the ullage heating component was 22 percent of the total. In all tests, the effect of the mass gain or loss in the test tank (due to unsteady tank pressure) was very small, from 0 to 2 percent of the total. Vacuum chamber pressure levels were similar in each of the tests, ranging from 3.0×10^{-4} to 6.7×10^{-4} Pa and averaged vacuum chamber wall temperatures (24 distributed locations) also were similar, ranging from 292 to 294 K. An analysis was performed on the vent line to estimate the contained vapor mass gain or loss due to temperature change. The vent line temperature effect was found to be negligible.

TABLE II.—SUMMARY OF BOILOFF TEST RESULTS

Test parameter	Test series		
	A	B	D
Fill level at end of test, percent	94	39	93
Pressure, MPa	0.61	0.58	0.61
Total time from start of back pressure control, hr	34.5	47.0	34.0
Elapsed time using flowmeter, hr	------	5.1	3.0
Elapsed time using weighing system, hr	11.3	8.0	8.0
Vent flowrate from flowmeter, kg/hr	------	1.55	1.61
Vent flowrate from weighing system, kg/hr	1.57	1.42	1.52
Total heating rate using flowmeter, W	------	106	95
Total heating rate using weighing system, W	92	98	92
Phase change component, percent	91	78	89
Ullage heating component, percent	8	22	9
Energy storage/release component, percent	2	0	2

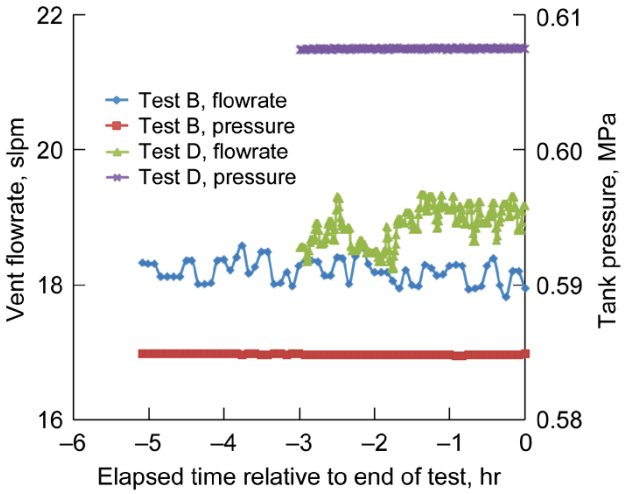

Figure 17.—Vent flowrate and tank pressure data used for boiloff analysis of Test Series B and D.

10.0 Thermodynamic Vent System Data Analysis

In this section, the methodology used to analyze the TVS data is explained.

10.1 Thermodynamic Vent System Cycle Time

A TVS cycle was defined to start when the vent valve was switched from an open to closed position. To ensure the start condition, the previous time step in the data file had to show that the vent valve was open. During a cycle, the following progression occurred:

(1) The vent valve closed at or near the cycle minimum (pressure or temperature).
(2) The vent valve remained closed as the liquid was heated and the tank pressure rose.
(3) The peak (temperature or pressure) condition was reached, and the vent valve was opened.
(4) The vent valve remained open as the liquid was cooled by operation of the TVS and the pressure dropped.
(5) The cycle was completed when the cycle minimum was reached. The vent valve closed, which coincided with the start of the next cycle.

In the data analysis, the open or closed status of the vent was determined from a reading of the TVS vent flowmeter. The vent valve was considered to be open whenever the vent flowmeter reading exceeded a threshold value. (The value was set at 1 percent of the meter's full-scale range to prevent erroneous open or closed classifications due to signal noise or to the slight offset observed during zero-flow conditions.) Although the vent valve required a finite time to open and close and the flowmeter also had a brief startup and shutdown response time, flowrate values between the no-flow and steady-flow values were very rarely recorded. The TVS cycle time was obtained by simply summing the time steps from the start to the end of a cycle. The individual cycle times within a group of similar successive cycles were arithmetically averaged to obtain the average cycle time, $\bar{t}_{\text{cycle}}$. The uncertainty in average cycle time is solely due to the uncertainty of the vent valve closing time, discussed shortly, and averaging over multiple cycles reduces this uncertainty per cycle. All uncertainties provided herein were estimated using the methods from Reference 17.

10.2 Thermodynamic Vent System (or Vent) Duty Cycle

The duty cycle of the TVS λ_{TVS} is the fraction of time that the TVS vent valve is open. This time was obtained by numerically integrating the TVS vent status over a complete cycle. The exact moment of valve opening was not recorded, so the trapezoidal rule was applied to the time step where the TVS vent status went from closed to open. The vent could open during the same time step as the pump startup or could be delayed by 1 to 2 time steps. Reported duty cycle values were arithmetically averaged over the available number of similar cycles.

The exact moment of vent closing was also not recorded, so the trapezoidal rule was applied here also (to the time step where the TVS vent status went from open to closed). Application of the rule was complicated by the simultaneous shutdown of the pump and the changing of the data-recording rate. If the recording rate was slowed down when the pump was turned off, then the shutdown had to occur within the first portion of the time step (equal to the shorter time step), and the shorter time step was used with the trapezoidal rule. The slowed-down recording rate was used in most of the tests. However, in some tests, the recording rate was increased when the pump was shut down and the vent closing could have occurred at any point within the time step. In either case, the correct time step to use was the shorter one.

Use of the trapezoidal rule can be viewed as numerically equivalent to assuming that the open/close events occur as step function changes at the midpoint of the time step; the timing uncertainties were thus equal to ±½ of the time step. The uncertainty in the total venting time of a TVS cycle was dominated by the uncertainties in the opening and closing times.

10.3 Pump Duty Cycle

The pump duty cycle λ_p is defined as the fraction of time that the pump was on (in operation). The elapsed time that the pump was on during a cycle was determined by numerically integrating the pump status (on/off) over a complete TVS cycle and dividing the result by the complete cycle time. The pump status was based on a measurement of the electrical power supplied to the pump's electrical controller. The data system's recording rate was determined by the pump status; the data system would switch the recording rate when the pump was started and would frequently interrupt (truncate) the previous time step. The uncertainty of the pump start time was negligible if an interruption was recorded; otherwise, the uncertainty was similar to the vent opening uncertainty. Pump shutdown always occurred at the same time as the vent valve closing discussed in Section 10.2; therefore, the numerical integration of the shutdown time step was identical. Because the pump was started prior to the delayed opening of the vent valve, the pump duty cycle was slightly greater than the TVS duty cycle. The uncertainty in the pump duty cycle was similar to the TVS duty cycle uncertainty.

10.4 Turnover Time

The liquid turnover time τ was calculated as the volume of liquid contained in the test tank divided by the pump's volumetric flowrate Ω_p:

$$\tau = \frac{FV_t}{\Omega_p} \tag{35}$$

Turnover time was used to gauge the time required to condition the liquid in the tank by simply flowing all the liquid through the heat exchanger. Use of the turnover time is admittedly an idealized situation because it assumes that all uncooled liquid is first drawn through the pump and heat exchanger without any mixing with cooled liquid discharged from the heat exchanger via the axial jet and/or spray hoops. For the test tank and pump used in the present study, τ = 0.65 hr at 90-percent fill and τ = 0.37 hr at 50-percent fill.

10.5 Vented Mass and Vent Flowrate

The instantaneous vent flowrate varied during a vent cycle and from cycle to cycle. As the tank pressure dropped during venting, the flowrate also dropped. Furthermore, if the TVS was operated in temperature-control mode, the tank pressure minimums and maximums dropped with each additional cycle. The amount of mass vented during a cycle was obtained by numerical integration (trapezoidal rule) of the flowrate readings over a complete cycle. For a number of similar cycles, an arithmetic average, $\overline{m}_{\text{vent}}$, was then calculated. The time-averaged vent flowrate per complete TVS cycle $\overline{\dot{m}}_{\text{cycle}}$ is useful for assessing the efficiency of the TVS performance and was calculated as

$$\overline{\dot{m}}_{\text{cycle}} = \frac{\overline{m}_{\text{vent}}}{\bar{t}_{\text{cycle}}} \tag{36}$$

The average vent flowrate $\overline{\dot{m}}_{\text{vent}}$, based only on the time the vent valve was open, is

$$\overline{\dot{m}}_{\text{vent}} = \frac{\overline{m}_{\text{vent}}}{\bar{t}_{\text{vent}}} = \frac{\overline{m}_{\text{vent}}}{\lambda_{\text{TVS}}\bar{t}_{\text{cycle}}} = \frac{\overline{\dot{m}}_{\text{cycle}}}{\lambda_{\text{TVS}}} \tag{37}$$

10.6 Heat Exchanger Performance

The instantaneous TVS heat exchanger heat removal rate $\dot{Q}_{HX}$ was calculated as

$$\dot{Q}_{HX} = \dot{m}_{vent}\left(h_{out} - h_{in}\right) \tag{38}$$

using the vent flowrate $\dot{m}_{vent}$ during the vent portion of the TVS cycle, the outlet enthalpy h_{out} of the vent flow downstream of the heat exchanger, and the vent flow inlet enthalpy h_{in} upstream of the J–T device. The vent flowrate was measured by the larger of the two flowmeters and the flowmeter data were converted using the methodology discussed in Section 5.0. The inlet enthalpy was based on the measured test tank pressure and measured temperature upstream of the J–T device. In some instances when the tank conditions were near saturation (as in Test Series A), the pressure and temperature values occasionally returned an enthalpy value for vapor. An inferred vapor phase was clearly not correct, because the inlet flow was liquid. The error resulted from very small measurement errors that were within the uncertainty specifications of the sensors. As an error-checking measure, the data analysis procedure also obtained the enthalpy for saturated liquid based on the inlet temperature. The procedure then used the lower of the two enthalpy values for the inlet.

The flow downstream of the J–T device was assumed to be two-phase and saturated. Thus, the downstream pressure was taken to be equal to the saturation pressure corresponding to the measured temperature downstream of the J–T device. (Noise in the downstream temperature measurement was small, less than the uncertainty of the measurement.) Furthermore, the pressure drop through the vent side of the heat exchanger was assumed to be zero. Modeling showed the vent-side pressure drop to be negligible (Ref. 18, personal communication). Therefore, the outlet pressure at the heat exchanger on the vent side was the same as the saturation pressure downstream of the J–T device. The vent flow outlet enthalpy could then be obtained by using the measured heat exchanger outlet temperature and pressure. The result was always superheated vapor, as expected for a well-designed heat exchanger.

The heat exchanger performance obtained from Equation (38) is an instantaneous value. The flowrate and various temperatures and pressures are not constant during a vent cycle and furthermore change from cycle to cycle. The instantaneous value was calculated for each recorded time interval. The total heat removed in each vent cycle was numerically evaluated using the trapezoidal rule (with the same assumptions as used for the venting time) to obtain the total heat removed in the cycle. Dividing this result by the total vent time t_{vent} gives the average heat removal rate $\overline{\dot{Q}}_{HX}$ for the vent portion of a complete TVS cycle:

$$\overline{\dot{Q}}_{HX} = \frac{\int_{t_{\text{vent}}} \overline{\dot{Q}}_{HX}\, \mathrm{d}t}{t_{\text{vent}}} \tag{39}$$

The average heat removal rate over a number of successive cycles was found by simple arithmetic averaging of the heat removal rates over the total number of available cycles. Note that this value was averaged over the venting periods only—not over the entire TVS cycle.

10.7 Quality Downstream of Joule-Thomson Device

The expansion at the J–T device was assumed to be isenthalpic (h = constant). The quality x of the two-phase flow downstream of the J–T device and also at the heat exchanger inlet (assuming that no heat transfer occurs between the J–T device and the heat exchanger) was calculated as

$$x = \frac{h_{in} - h_f}{h_{fg}} \tag{40}$$

where h_f and h_{fg} are saturated properties at the downstream pressure. All other things being equal, a low value is desirable because it indicates greater capacity for heat removal as the vent flow is vaporized in the heat exchanger.

10.8 Energy Balance Applied to a Complete Thermodynamic Vent System Cycle

An overall energy balance on the test tank using a control volume approach was applied using data for each temperature-controlled test segment. This energy balance provides a check on the consistency of the test results. If constant temperature is assumed, the change in the propellant internal energy is due to the change in fill level and the change in helium internal energy is negligible. The vented mass is known, and depending on the choice of the control volume boundary, the exiting mass at the vent is either liquid if the J–T device and heat exchanger are outside the boundary or vapor if they are inside the boundary. If the heat exchanger is at the boundary of the control volume, then the heat exchange at the heat exchanger is included in the energy balance. The energy input due to environmental heating is approximately known from the boiloff tests, and the TVS and pump duty cycles are known. The remaining component in the overall balance is the energy input due to pump power dissipation. The energy balance can be solved for this and the result compared to the specification for the pump provided by the manufacturer. The two forms of the energy balance gave nearly identical results so only the vapor venting model is discussed.

If the TVS heat exchanger is within the control volume and vapor exits the control volume at the liquid temperature and vent pressure,

$$\dot{Q}_p = \frac{\dfrac{U_2 - U_1}{t_{\text{cycle}}} - \dot{Q}_e + \dfrac{m_{vent}\, h(T,P)}{t_{\text{cycle}}}}{\lambda_{\text{p}}} \tag{41}$$

where the subscript p refers to the pump.

10.9 Thermodynamic Vent System Efficiency

VanOverbeke (Ref. 6) defines a TVS efficiency η as the ratio of the boiloff rate $\overline{\dot{m}}_o$ to the time-averaged TVS vent flowrate $\overline{\dot{m}}_{\text{cycle}}$ for the same tank system:

$$\eta = \frac{\overline{\dot{m}}_o}{\overline{\dot{m}}_{\text{cycle}}} \tag{42}$$

Equation (42) is an attractively simple figure of merit, but the comparison can be distorted by variations in ullage conditions. If one recalls Equation (32), the boiloff rate for a given tank heating rate depends on the fill fraction. That is, the boiloff flowrate decreases as the fill fraction is reduced because a greater fraction of the heat input is directly absorbed by the vapor rather than contributing to liquid vaporization. From the present boiloff results (Table II), ullage superheating was 8 to 9 percent of the total heating at a fill fraction of 0.93 to 0.94 and 22 percent of the total heating at a fill fraction of 0.39. What happens in the ullage also impacts the efficiency of the TVS: an axial jet system in normal gravity with increasing unwetted wall temperatures will have a lower vent flowrate than a system that maintains a cold unwetted tank wall region because less energy is removed by the TVS in the former case.

10.10 Thermodynamic Vent System Test Results

The TVS tests were conducted with differing hardware configurations and test conditions as summarized in Table I. A more detailed tabulation of the test conditions (test segment identification (I.D.), test fluid, control logic mode, number of cycles, total test time, median pressure, median liquid temperature, median vent pressure, median fill fraction, and average vacuum level) is given in Table III. Median values (average of observed minimum and maximum values) are useful for conditions where the sawtooth TVS profiles trended upward or downward over multiple cycles. Key results of the data analysis (cycle time, pump and TVS duty cycles, vented mass per cycle, vent flowrate (when vent was open), and cycle-averaged vent flowrate) are listed in Table IV along with estimated uncertainties for various parameters. Other TVS test results (heat exchanger heat removal rate, quality downstream of the J–T device, turnover time, and TVS efficiency) are presented in Table V. These results are all discussed in Sections 11.0 and 12.0.

TABLE III.—DETAILED SUMMARY OF THERMODYNAMIC VENT SYSTEM (TVS) TEST CONDITIONS

Test	Fluid	Logic mode[a]	Number of cycles	Total test time, hr	Median pressure, MPa	Median temperature, K	Median vent pressure, MPa	Median fill fraction	Average vacuum level, Pa
90A_1	O_2	Combined	3	9.7	0.60	111.3	0.24	0.87	6.0×10^{-4}
50A_1		Combined	2	27.7	.57	110.5	.25	.49	4.8
90B_1		*T* control	7	14.6	1.47	111.6	.12	.88	5.5
50B_1		*T* control	13	18.3	1.62	111.3		.46	5.1
50B_2		*P* control	13	15.8	1.60	111.9		.43	5.1
90C_1		*T* control	9	23.4	1.40	111.5		.87	4.7
90C_2		*P* control	3	13.0	1.32	112.0		.85	4.1
50C_1		*T* control	9	18.3	1.60	111.5		.50	5.1
50C_2		*P* control	4	9.3	1.57	111.7		.48	4.7
50C_3		*T* control	6	12.2	1.52	111.5		.46	4.1
90D_1			6	16.7	1.47	111.5		.86	3.5
90D_2			3	8.1	1.36	111.9		.84	
50D_1			8	20.8	1.63	111.6		.51	2.9
50D_2		*P* control	3	11.0	1.61	111.8		.49	3.3
50D_3		*T* control	3	7.8	1.60	112.1		.48	3.1
50E_1	N_2	*T* control (with added GHe)	4	5.0	1.59	100.0	.11	.48	8.5
50E_2		*T* control	11	13.8	1.57	100.0		.45	6.4
50E_3		*T* control (with added GHe)	5	6.3	1.58	100.0		.42	6.4
50E_4		*P* control	13	15.0	1.59	100.3		.40	5.5

[a]*T*, temperature, or *P*, pressure.

TABLE IV.—DETAILED SUMMARY OF THERMODYNAMIC VENT SYSTEM (TVS) TEST RESULTS (PART 1)

Test	Average cycle time, hr	Uncertainty cycle time, percent	Pump duty cycle	TVS duty cycle	TVS duty cycle uncertainty	Average vented mass per cycle, kg	Vent flowrate, kg/hr	Uncertainty in average vented mass per cycle, percent	Cycle-averaged vent flowrate, kg/hr	Uncertainty of cycle-averaged vent flowrate, percent
90A_1	3.2	±0.2	0.70	0.69	±0.01	8.8	4.0	±4	2.7	±4
50A_1	13.9	±0.1	.74	.74	±0.00	36.1	3.5	±5	2.6	±5
90B_1	2.1		.21	.20	±0.01	4.6	10.9	±5	2.2	±5
50B_1	1.4		.18	.17		2.8	11.5	±7	2.0	±7
50B_2	1.2		.15	.14		1.9	11.7	±11	1.6	±11
90C_1	2.6		.24	.24		6.4	10.3	±3	2.5	±3
90C_2	4.3		.14	.14	±0.00	5.7	9.8	±4	1.3	±4
50C_1	2.0		.22	.22	±0.01	5.1	11.6	±4	2.5	±4
50C_2	2.3	±0.2	.18	.17		4.6	11.4	±5	2.0	±5
50C_3	2.0	±0.1	.22	.22		4.9	11.1	±5	2.4	±5
90D_1	2.8	±0.1	.20	.20		5.9	10.7	±4	2.1	±4
90D_2	2.7	±0.2	.22	.21		5.8	10.1		2.1	
50D_1	2.6	±0.1	.18	.18		5.3	11.5		2.0	
50D_2	3.7	±0.2	.14	.14	±0.00	5.9	11.4		1.6	
50D_3	2.6	±0.2	.19	.19	±0.01	5.5	11.3		2.1	
50E_1	1.2	±0.4	.43	.42		4.6	8.8		3.7	
50E_2	1.3	±0.1	.35	.35		3.7	8.6	±3	3.0	±3
50E_3	1.3	±0.2	.32	.31		3.4	8.7	±4	2.7	±4
50E_4	1.2	±0.1	.25	.24		2.4	8.6	±5	2.1	±5

TABLE V.—DETAILED SUMMARY OF THERMODYNAMIC VENT SYSTEM (TVS) TEST RESULTS (PART 2)

Test	Logic mode[a]	Heat exchanger (HX) heat removal rate, W	Uncertainty in HX heat removal rate, percent	Average quality (J–T exit)	Tank turnover time, hr	Pump-on-time to turnover-time ratio	TVS efficiency
90A_1	Combined	213	±4	0.10	0.63	3.61	0.67
50A_1	Combined	189	±5	.10	.36	29.05	.69
90B_1	*T* control	586	±5	.16	.64	.70	.83
50B_1	*T* control	626	±8	↓	.33	.77	.90
50B_2	*P* control	633	±11	↓	.31	------	----
90C_1	*T* control	561	±4	↓	.63	1.00	.74
90C_2	*P* control	529	±4	.17	.61	------	----
50C_1	*T* control	624	±5	.16	.36	1.25	.73
50C_2	*P* control	615	±5	↓	.34	------	----
50C_3	*T* control	602	±5	↓	.33	1.35	.76
90D_1	↓	580	±4	↓	.62	.90	.85
90D_2	↓	545	±4	.17	.61	.97	.85
50D_1	↓	620	±5	.16	.37	1.30	.89
50D_2	*P* control	619	±4	.16	.35	------	----
50D_3	*T* control	609	↓	.17	.34	1.43	.87
50E_1	*T* control (with added GHe)	423	↓	.24	.34	1.55	----
50E_2	*T* control	414	↓	↓	.33	1.35	----
50E_3	*T* control (with added GHe)	421	↓	↓	.31	1.31	----
50E_4	*P* control	415	±5	↓	.29	------	----

[a]*T*, temperature, or *P*, pressure.

When tests were conducted at more than one fill level, the higher fill level was tested first; then the test tank was drained to the lower fill level of the second test. For each of the test segments, a figure showing the resulting temperature and pressure cycles is provided (Figs. 18, 21, 25, 27, 30, 34, 38, 41, and 43). The entire histories are shown, with unanalyzed regions in lighter grey and the analyzed portions of the curve in darker colors. The tank pressure and average liquid temperatures used in the detailed analyses are shown. For each test, a second figure is provided that shows the measured liquid temperatures at a few selected locations from near the tank bottom to just below the liquid free surface (Figs. 19, 22, 26, 29, 31, 35, 39, 42, and 44). In these figures, the plotted liquid temperature is a centered 11-point running average (average of 11 measurements in time—five before and five after the plotted time). This was done to remove scatter due to signal noise. In addition, the curves are slightly adjusted with small temperature offsets to force the curves to align vertically, thus allowing easier visual comparison of the results. The temperature offsets are very small, much less than the tolerance bands specified by the sensor manufacturer, and are the same for each figure. The temperature range of these figures also is small; using the offsets greatly improves clarity. The data in the figures showing liquid temperatures from near the tank bottom to just below the liquid free surface (Figs. 19, 22, 26, 29, 31, 35, 39, 42, and 44) are for up to six consecutive cycles observed during temperature-controlled TVS logic (if pressurized with GHe).

Finally, some figures (Figs. 20, 23, 32, and 36) show a few examples of the temperatures near the liquid-ullage interface, and other figures (Figs. 24, 33, 37, and 45) show the ullage, tank lid, and unwetted tank wall temperatures observed in some of the tests. Only a few representative examples are provided because the results were often similar for various tests.

11.0 Discussion of Results for Each Individual Thermodynamic Vent System Test

11.1 Test 90A

The LO_2 was saturated at the total tank pressure of about 0.6 MPa and saturation temperature of 111 K; no GHe pressurant was present. The pump discharge was routed through the axial jet. Plots of the tank pressure and average liquid temperature are shown in Figure 18. After the initial period of about 13 hr in which the TVS heat exchanger was operated extensively, three complete cycles were performed with a 0.034-MPa pressure-control band. There was a rapid pressure drop early in the vent cycle, attributed to breakup of

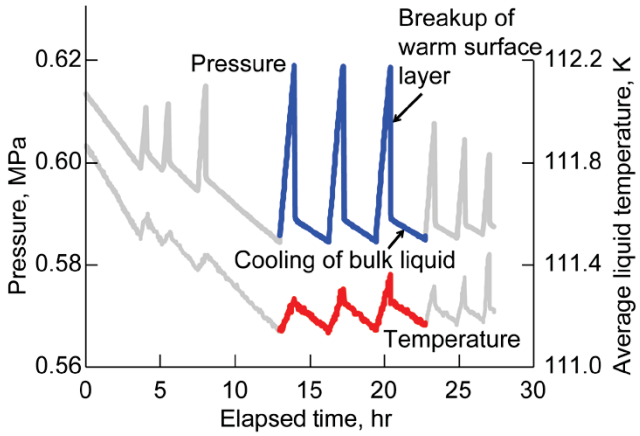

Figure 18.—Tank pressure and average liquid temperature for Test 90A.

the warm thermal layer at the liquid surface by the axial jet flow. The initial pressure reduction was far larger than for any other tests in the present work and was attributed to the augmented thermal stratification at the liquid-vapor interface because of the absence of helium (liquid was not subcooled) and the high fill level (enhanced free convection due to tall wetted sidewall heating). The remaining pressure drop during the vent cycle occurred as the heat exchanger cooled the bulk liquid, reducing the temperature and the corresponding saturation pressure. As expected, the liquid temperature cycles were well synchronized with the pressure cycles. The results demonstrate the TVS's ability to control tank pressure and liquid temperature.

The test pressure for Test Series A was far below the TVS design point, so the heat exchanger performance was substantially reduced for Test Series A because of the low vent flowrate of 4 kg/hr. During the vent cycle, the averaged heat removal rate of the TVS was 213 W (compared with the design point of about 600 W), requiring a high duty cycle of 0.69. Also, the average liquid temperature signal was noisy, as seen in Figure 18. Once the noise was observed, efforts were begun to modify the data system software. Furthermore, the TVS cycles were lengthier than desired if the test schedule was to be maintained. Because the goal was to demonstrate 6 to 10 cycles per test, it was necessary to reduce the control band for pressure (or temperature). When control with a narrower band was attempted (beginning at 23 hr), variations in the cycle peaks were apparent. Some of the variability was attributed to the noise in the temperature and pressure signals, as well as to some of the delay times in the control logic being too long.

As seen in Figure 19, there was little difference in liquid temperatures at various heights within the liquid. At all sensor locations, the liquid temperature responded in a nearly identical manner to the pressure cycle. Although the figure indicates that temperature maximums and minimums increased with time, the increase was on the order of only a few

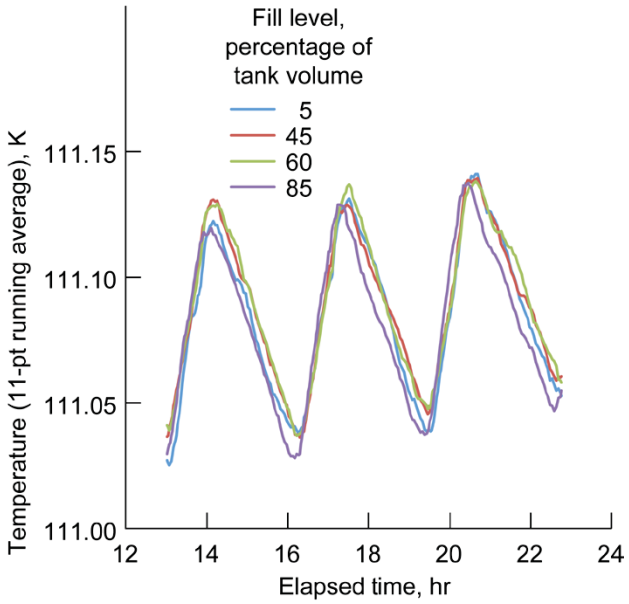

Figure 19.—Liquid temperatures during Test 90A thermodynamic vent system (TVS) cycles.

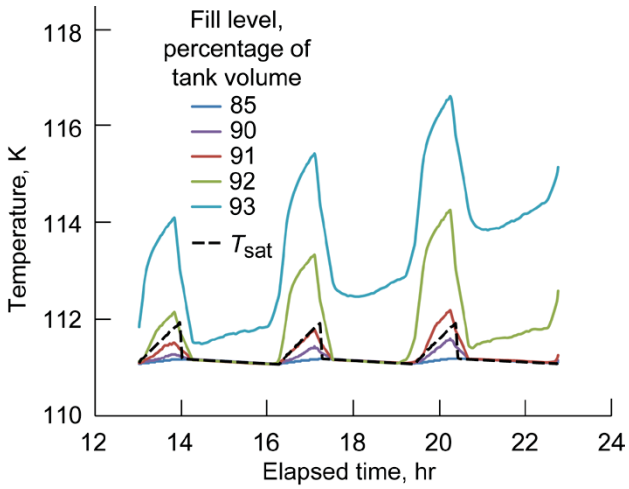

Figure 20.—Liquid-ullage interface temperatures during Test 90A thermodynamic vent system (TVS) cycles; T_{sat}, temperature of saturated vapor.

hundredths kelvin. The author does not consider this increase to be significant because of the signal noise and logic delay time issues mentioned in Sections 6.0, 7.0, and 10.1. The axial jet configuration did not provide ullage and unwetted wall thermal control capability in the normal-gravity test environment. Although not shown, the tank lid and ullage temperatures increased steadily throughout the test. Figure 20 shows the thermal stratification near the liquid-ullage interface. The temperature sensor at 93-percent fill was clearly in the ullage for all TVS cycles shown. The sensor at 92-percent fill appeared to be initially in the liquid, but it was in the ullage during the last cycle shown, thus indicating that the liquid level had dropped due to TVS venting. The dashed

line in the figure is the saturation temperature obtained from the tank pressure measurement. The saturation temperature should represent the temperature of the liquid-ullage interface of a fluid system containing only pure liquid and vapor. The maximum-to-minimum saturation temperature difference (or maximum liquid thermal stratification) for these TVS cycles was slightly less than 1 K. The peak temperature measured by the sensor at 90-percent fill increased with successive TVS cycles as the liquid level dropped and became closer to the sensor's position.

11.2 Test 50A

Test 50A was conducted at about 50-percent fill and without GHe pressurant. The pressure and liquid temperature cycles are shown in Figure 21. Two complete cycles were obtained from 11 to 40 hr. The duty cycle of 0.74 and heat exchanger performance of 189 W are similar to those for Test 90A, as expected. The slightly larger duty cycle and slightly lower heat removal rates are due to the average tank pressure being lower than for the previous test (0.57 vs. 0.60 MPa). Although the pressure control band is the same as for Test 90A and the duty cycle is about the same, the cycle time is much greater (13.9 vs. 3.2 hr). Comparing Figures 18 and 21 shows that the pressure rise rate was much slower at 50-percent fill than at 90-percent fill and that the pressure drop due to the mixer-operation-only prior to TVS venting was less. Both results from the comparison indicate that less thermal stratification developed in each cycle at the lower fill level. The cycle control band (pressure or temperature) would have to be reduced to obtain the desired number of cycle repeats for the given test schedule. When control with a narrower band was attempted, beginning at 42 hr, the noisy temperature signal was clearly not acceptable and noise in the pressure signal also became apparent.

Figure 22 shows the cyclic behavior of the liquid temperature at various fill locations. The response was nearly identical at each sensor location, and the variations in the minimums and maximums are again thought to be insignificant. A key difference for Test 50A was the much larger liquid maximum-to-minimum temperature swing per cycle. It was about 0.5 K for Test 50A in comparison to 0.15 K for Test 90A. The reduced wetted sidewall height for Test 50A resulted in less warm liquid accumulation at the liquid-vapor interface, a longer heating period, and reduced pressure drop during the initial portion of the mixing/vent cycle. The total cycle time for Test 50A was substantially longer than for any other tests reported herein. Figure 23 shows measured temperatures near the liquid-ullage interface. An interesting observation for Test 50A is the significant drop in liquid level from the first to second TVS cycle, as shown. The sensor at 60-percent fill was clearly in the ullage during both cycles. The sensors at 55-, 54-, and 53-percent fill were submerged in the liquid during the first cycle and then exposed to the ullage in

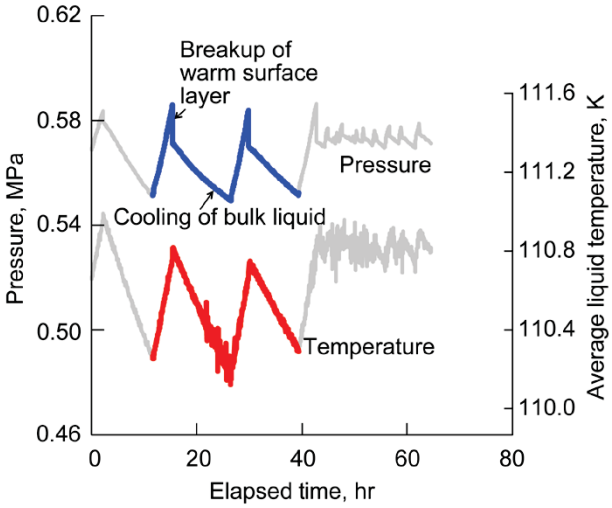

Figure 21.—Tank pressure and average liquid temperature for Test 50A.

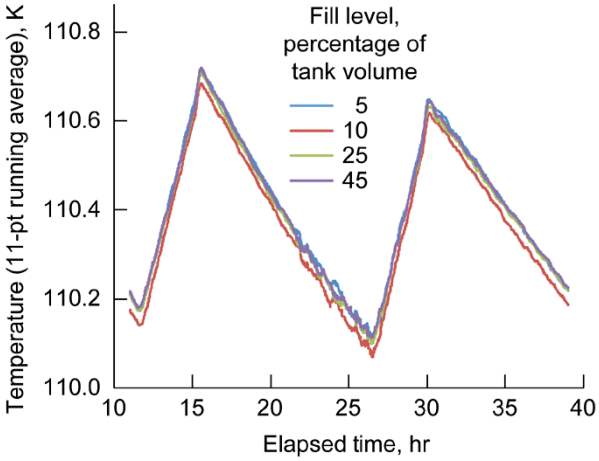

Figure 22.—Liquid temperatures during Test 50A thermodynamic vent system (TVS) cycles.

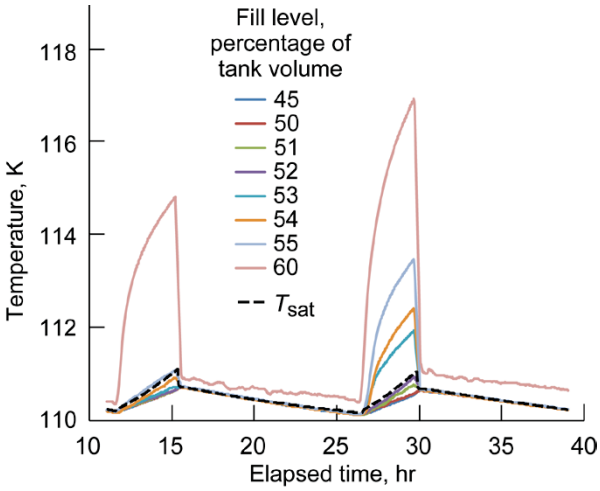

Figure 23.—Liquid-ullage interface temperatures during Test 50A thermodynamic vent system (TVS) cycles; T_{sat}, temperature of saturated vapor.

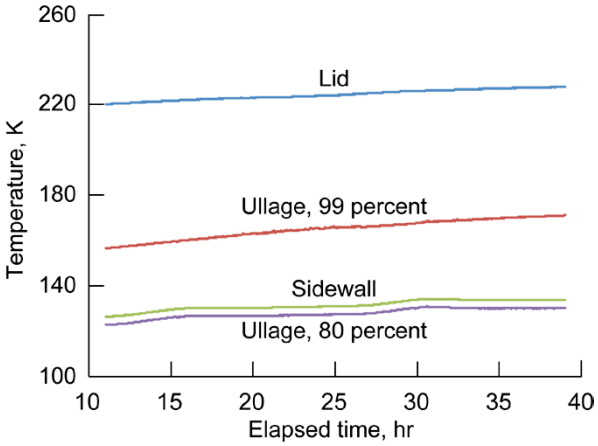

Figure 24.—Ullage, lid, and unwetted wall temperatures during Test 50A.

the second cycle. The maximum thermal stratification in the liquid, as denoted by the saturation temperature curve, was slightly less than 1 K, which is similar to the result at 90-percent fill, but for a much longer cycle time (13.9 vs. 3.2 hr).

Figure 24 shows that the tank lid, ullage, and unwetted wall temperatures rose steadily during Test 50A, as one might expect with an axial jet mixer in normal gravity. At the conclusion of Test 50A, data system software with the enhanced signal-conditioning features described in Section 7.0 was ready for use for all remaining test series. Both tests for the Test Series A demonstrated the linked behavior of the pressure and temperature cycles for a tank with a single component (pure vapor) ullage. The axial jet mixer appeared to mix the liquid contents well, but in normal gravity, it did not control ullage or unwetted wall temperatures.

11.3 Test 90B

Test Series B used the same axial jet hardware configuration as Test Series A. The LO_2 temperature was again about 111 K, but the tank was pressurized with GHe to a total tank pressure of about 1.5 to 1.6 MPa. Test 90B conducted at approximately 90-percent fill resulted in three sets of temperature control cycles, with GHe repressurization after the first and second sets. Much of the initial pressure drop after pressurization or repressurization was attributed to cooling (pressure collapse) of the warm GHe pressurant when it was introduced into the colder test tank. Figure 25 shows the pressure and temperature cycles. Two key results are readily seen. First, the signal conditioning worked well, resulting in clean, repeated cycles. A larger number of cycles were successfully completed in a shorter timeframe, roughly a cycle every 2 hr. Second, the pressure slowly dropped with each cycle repeat while the liquid temperature was controlled within the lower and upper set points, as expected based on the thermodynamic model presented in Section 1.2.

The third set of TVS cycles was analyzed, with the results summarized in Tables III to V. The test conditions were near

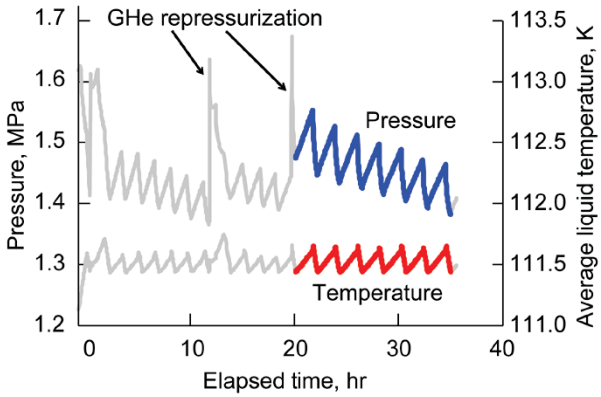

Figure 25.—Tank pressure and average liquid temperature for Test 90B; GHe, gaseous helium.

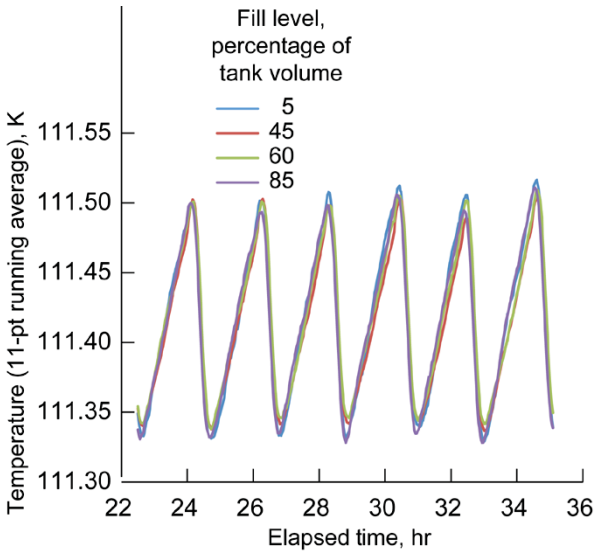

Figure 26.—Liquid temperatures during Test 90B thermodynamic vent system (TVS) cycles.

the TVS heat exchanger design point as reflected by a duty cycle of 0.20 and a heat exchanger performance of 586 W. Because the tank pressure was much higher than for Test Series A, the vent flowrate was much higher (10.9 vs. 3.5 to 4.0 kg/hr). The temperature control band was 0.17 K with a corresponding 0.08 MPa swing in pressure. The recorded temperature swing was slightly greater because of a small upward spike in temperature at mixer startup. The cause was not investigated, but the spike may have been due to rapid vaporization of cold liquid being pumped through external valves and lines that had warmed up while the pump was off. As shown in Figure 26, the temperatures were again very uniform at the various sensor locations within the ullage. Although not shown, the tank lid and ullage temperatures for Test 90B slowly increased throughout the test. The lid and ullage temperatures were significantly higher than the liquid temperature because the axial jet (in a normal-gravity environment) was unable to cool these locations.

11.4 Test 50B

Test 50B followed Test 90B, after which the tank was drained to ~50-percent fill, exposing the cold upper tank sidewall to the ullage. The tank was then repressurized with GHe. In Test 50B, the upper tank wall, tank lid, and ullage temperatures increased throughout the test. As the unwetted tank sidewall warmed up, the ullage temperature rose as well, which in turn increased the partial pressure of the GHe. The ullage warming effect was opposed by the operation of the TVS, which decreased the GHe partial pressure by expanding the ullage. Initially in Test 50B, the ullage warming effect appeared to dominate. Eventually a tipping point was reached (as shown in Fig. 27) after 30-plus hours of operation, and the tank pressure decreased while operating the TVS in temperature control mode. The observed normal-gravity tank pressure behavior in Test 50B could be different from what would occur in low gravity.

A portion of the data from Figure 27 is magnified in Figure 28, where seven complete TVS cycles under temperature-controlled logic are shown. The temperature maximums and minimums were stable, whereas the pressure cycles exhibited a repeatable cyclic behavior with a declining trend of pressure. The liquid temperature distribution is shown in Figure 29 and is similar to the axial jet test results presented in Section 11.3.

After demonstrating that the TVS could reduce tank pressure using temperature-control logic, a second test with pressure-control logic was performed. Test 50B was the first test to implement pressure-control logic with GHe in the tank. As seen in Figure 27, beginning at 65 hr, the tank pressure was kept within the pressure-control set points and the average liquid temperature increased as expected, based on model predictions. The duty cycles and the cycle-averaged vent flowrate were lower under pressure control than under temperature control because less energy removal is required (via TVS venting) when the tank and liquid are permitted to warm up.

11.5 Test 90C

In Test Series C, the pump discharge was split, with an unknown portion routed through the axial jet and the remainder through the two spray hoops near the top of the tank. For the approximate 90-percent fill test, about four temperature-controlled cycles were initially completed. Then the test tank was repressurized, and the TVS was operated uninterrupted in temperature-control mode from about 15 to 40 hr, as shown in Figure 30. After that, the control logic was switched to pressure control for three cycles. The same trend was observed, as seen before in Test 50B under pressure control: the liquid temperature rose while the pressure cycled within the control band.

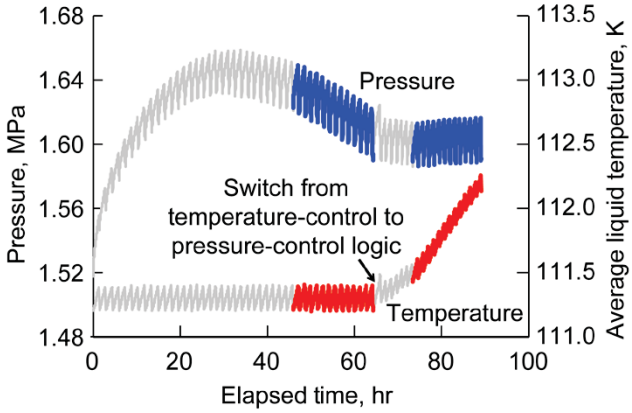

Figure 27.—Tank pressure and average liquid temperature for Test 50B.

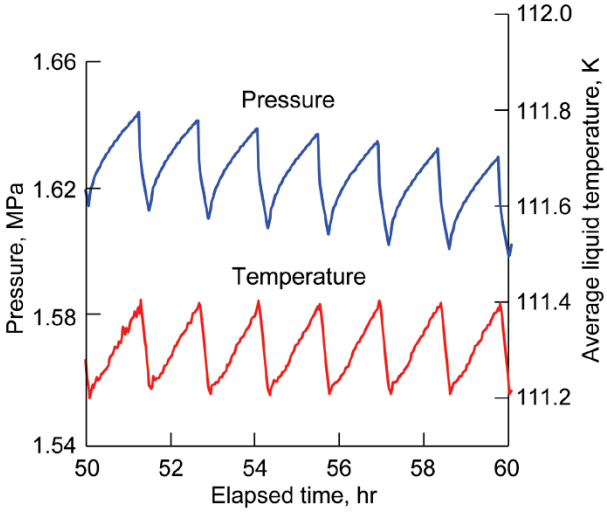

Figure 28.—Closeup of seven temperature-controlled pressure and temperature cycles for Test 50B.

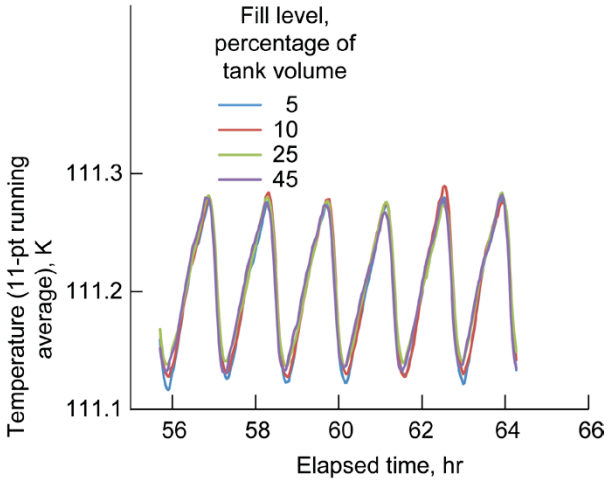

Figure 29.—Liquid temperatures during Test 50B thermodynamic vent system (TVS) cycles.

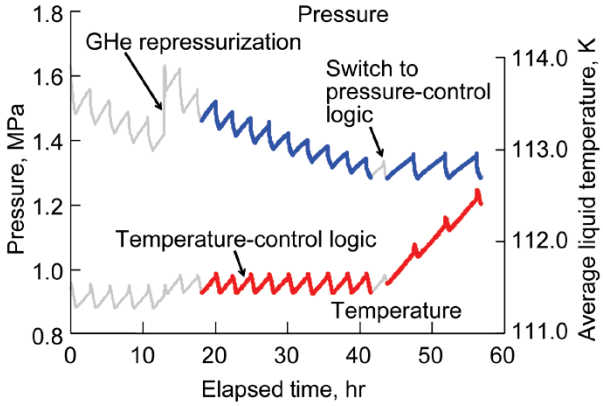

Figure 30.—Tank pressure and average liquid temperature for Test 90C.

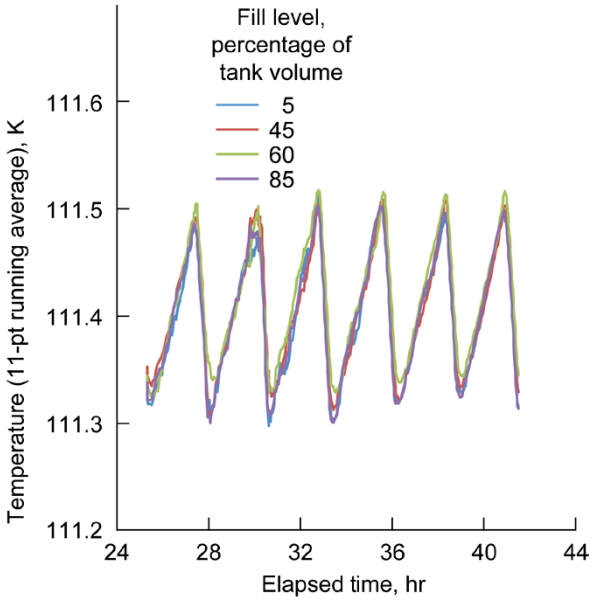

Figure 31.—Liquid temperatures during Test 90C thermodynamic vent system (TVS) cycles.

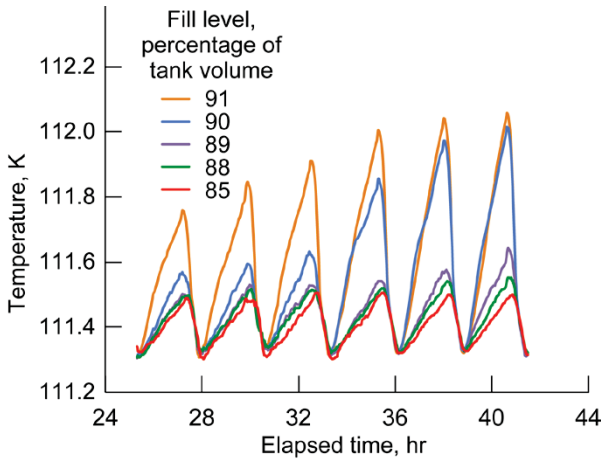

Figure 32.—Liquid-ullage interface temperatures during Test 90C thermodynamic vent system (TVS) cycles.

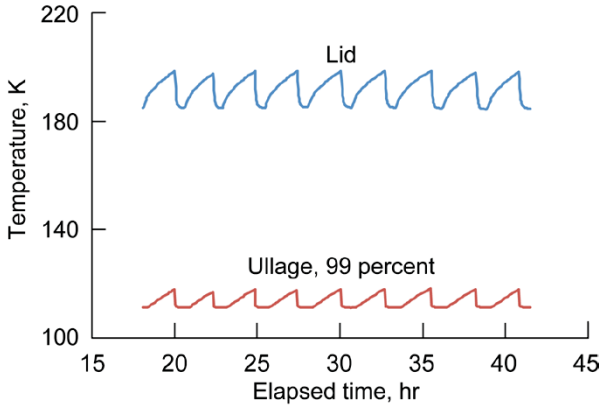

Figure 33.—Ullage and lid temperatures during Test 90C.

Figure 31 shows a sample of the liquid temperature behavior. The plot looks very similar to those seen in the previous axial jet tests, but with an indication of some short-term randomness at the individual locations. The randomness could be caused by the diminished strength of the axial jet flow because some of the pump discharge was going through the spray hoops. Figure 32 shows the measured temperatures near the liquid-ullage interface. The sensor at 91-percent fill appears to have been in the ullage for all cycles. The sensor at 90-percent fill was initially in the liquid (or very near the liquid) but was in the ullage at the end of the cycles. The sensor at 89-percent fill may have become exposed to the ullage during the last cycle. The temperature scale was much smaller than in the similar figures for Test Series A (pure liquid and vapor). Also, the temperatures on the liquid side of the interface were essentially the same as for the bulk liquid (the 85-percent sensor reading is also used in Fig. 30). Therefore, there was minimal thermal stratification in the liquid. The reduction in stratification may have been partially due to the shorter cycle time in comparison to Test Series A, but it was more likely due to the presence of helium in the ullage and the resulting subcooled liquid.

Figure 33 confirms flow through the spray hoops. The lid temperature, measured by a thermocouple on the outside surface of the lid cyclically varied as the pump was turned on and off. The silicon-diode sensor located at the 99-percent fill location warmed when the pump was off and cooled to the liquid temperature (111 K) when the pump was on. The minimums and maximums of both sensors were steady over time, indicating the ability of the spray hoops to control ullage and lid temperatures and maintain steady-state thermal conditions. The lid temperature remained under 200 K for Test 90C; whereas in the axial-jet-only tests, the lid temperature was higher (e.g., ~220 K in Fig. 24, Test 50 A).

11.6 Test 50C

Smooth operation of the TVS was demonstrated in Test 50C, as shown in Figure 34. Nine temperature-controlled cycles were conducted first, followed by four pressure-controlled cycles. Then the control logic was switched back to the initial temperature-control set points. Because the liquid temperatures had increased during the pressure-controlled operation, the TVS had to vent steadily for a longer time to cool the liquid and return to the minimum-temperature set point. Once the minimum set point was reached, the TVS operated through six more temperature-controlled cycles. The cycle times, duty cycles, and vented mass for the first and third segments (both temperature-controlled) are very similar as seen in Table IV. In Figure 35, occasional short-term randomness in the liquid temperature at various locations again occurred. Otherwise, the behavior is very similar to that seen when the entire pump discharge was routed through the axial jet.

Figure 36 shows the liquid-ullage interface temperatures. Results are similar to the Test 90C results discussed in Section 11.5. The drop in liquid level is apparent because the temperature at 52 percent rose when the sensor was exposed to the ullage. Again, there was very little thermal stratification on the liquid side, which the author attributes to the shorter cycle times and liquid subcooling due to helium pressurization.

The effect of the spray hoops is evident in Figure 37. The lid temperature cycled as the pump was turned on and off, as did the ullage temperature at the 99-percent fill location. Two additional temperatures are shown, both closer to the liquid surface. The sidewall temperature shows a very slight cyclic oscillation as does the ullage temperature at the 80-percent fill location. Both ullage temperatures dropped to the liquid temperature (111 K) when the pump was running. The long-term trend is one of steady cyclic oscillations, thus indicating the ability of the spray hoops to control and maintain the thermal conditions in the upper tank region.

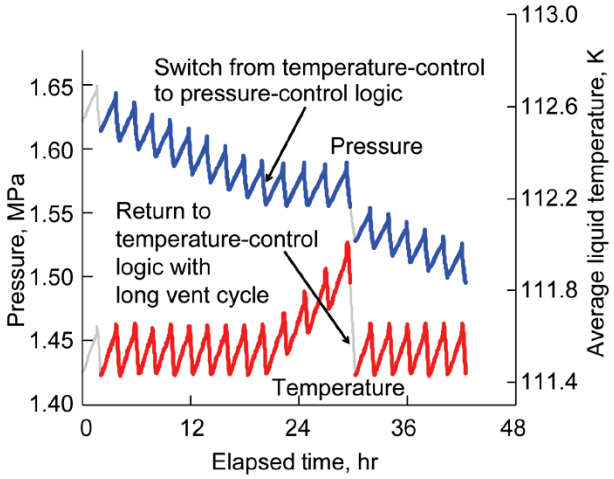

Figure 34.—Tank pressure and average liquid temperature for Test 50C.

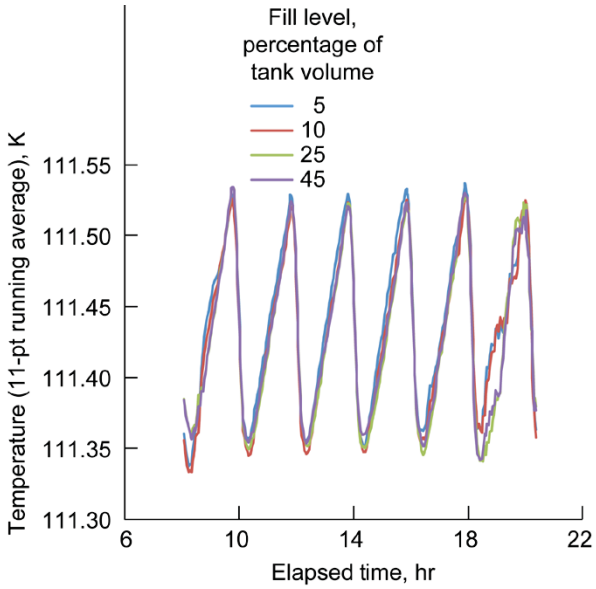

Figure 35.—Liquid temperatures during Test 50C thermodynamic vent system (TVS) cycles.

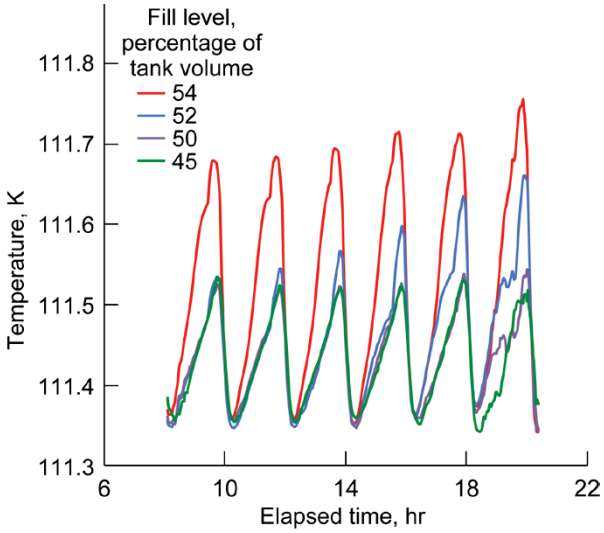

Figure 36.—Liquid-ullage interface temperatures during Test 50C thermodynamic vent system (TVS) cycles.

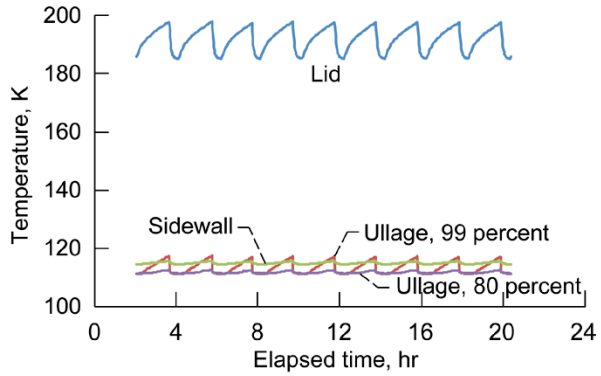

Figure 37.—Ullage, lid, and unwetted wall temperatures during Test 50C.

11.7 Test 90D

In Test Series D, all pump discharge flow was routed through the spray hoops in the ullage. The test at ~90-percent fill started with temperature-controlled TVS cycles, which were executed successfully. When control was switched to pressure-controlled logic, a few pressure cycles were obtained, but the average liquid temperature climbed steadily, as seen in Figure 38. The attempt at pressure control in Test 90D was the only occurrence in the entire test program where the TVS did not operate successfully. The unsuccessful result was not totally unexpected because active mixing of the liquid was due solely to liquid intake at the pump inlet and droplets falling on the liquid surface. Results may have been different if a wider pressure control band were tried. However, no further testing was attempted with pressure control at 90 percent. A second segment of temperature-controlled cycles was then performed.

Figure 39 shows the liquid temperatures for six representative temperature-controlled cycles. The results are clearly a bit different from any of the previous tests. The temperatures are still cyclic and repeat themselves quite well, but the upper locations show upward spikes when the pump is started (at the cycle peaks) and the bottom location shows an unusual lower minimum. The temperature at 5-percent fill seems to have twice the amplitude of the temperature at 45 percent, but there is no overall long-term divergence or convergence of the measured liquid temperatures. The lid and ullage temperatures for Test 90D were very similar to those for Test 90C. Performance specifications are given in Tables IV and V. Duty cycles and vented mass are slightly lower than for the combined axial jet and spray hoops test (Test 90C).

Figure 40 provides more detail about the pressure-controlled portion of Test 90D. During the first self-pressurization period, the liquid temperatures became equal and increased at the same rate. Just before the first cycle peak, some thermal stratification began to develop. The first and second vent cycles did not destratify the liquid because the thermal gradient from 5- to 85-percent fill persisted. The third vent cycle with a greater pressure drop (the set points were changed and the control logic switched to temperature control as the vent cycle was in progress) shows both a temperature reduction and some destratification. The incomplete destratification was not seen in other tests and is an indication that spray-hoops-only configuration was not totally effective in mixing the liquid sufficiently to achieve isothermal conditions.

11.8 Test 50D

Next, the tank was drained to 50 percent, and the spray-hoops-only configuration was tested first with temperature control logic, then with pressure control, and finally with temperature control again. The TVS appeared to

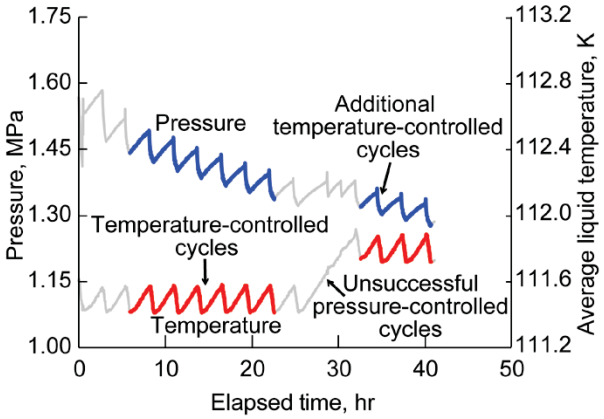

Figure 38.—Tank pressure and average liquid temperature for Test 90D.

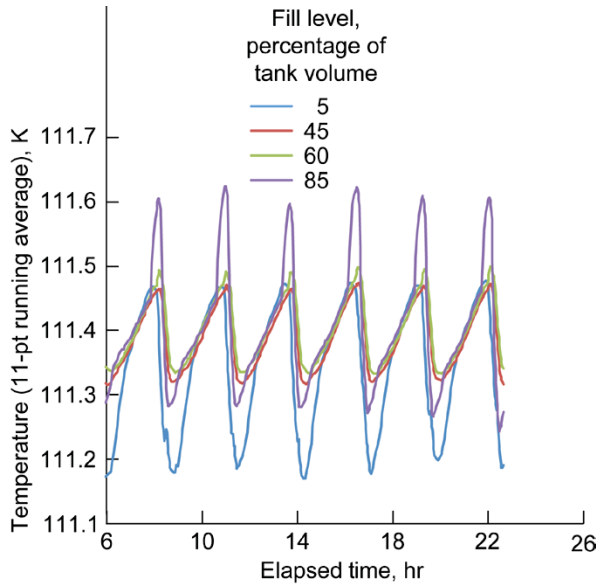

Figure 39.—Liquid temperatures during Test 90D thermodynamic vent system (TVS) cycles.

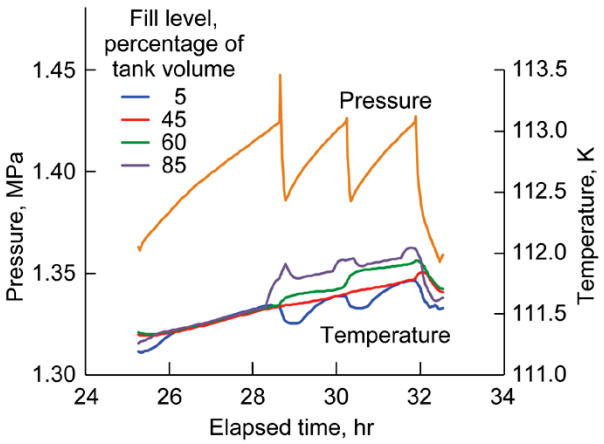

Figure 40.—Pressure and liquid temperatures for pressure-controlled operation in Test 90D.

perform satisfactorily in each segment. Figure 41 shows the pressure and liquid temperature cycles, and Figure 42 shows the individual temperature histories for six representative liquid locations. The trends are similar to those seen with the same hardware configuration at 90-percent fill (Test 90D). The upper sensors show a temperature spike where the pump turned on. The spike might have been caused by warmer liquid falling on the liquid surface as a result of spray droplet contact with the tank lid and upper tank wall. The lowest sensor shows a wide peak-to-peak swing in temperature. There does not seem to be any long-term divergence or convergence of the temperature cycles; the cyclic results look repeatable and consistent. Table III shows similar performance results for the two temperature-controlled test segments. The duty cycles and vented mass are slightly lower than for Test 90D.

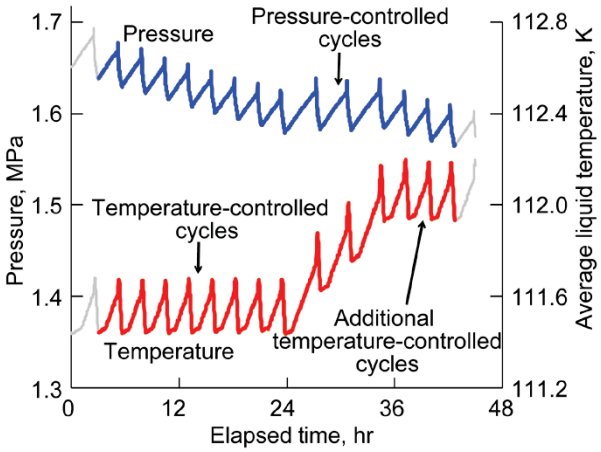

Figure 41.—Tank pressure and average liquid temperature for Test 50D.

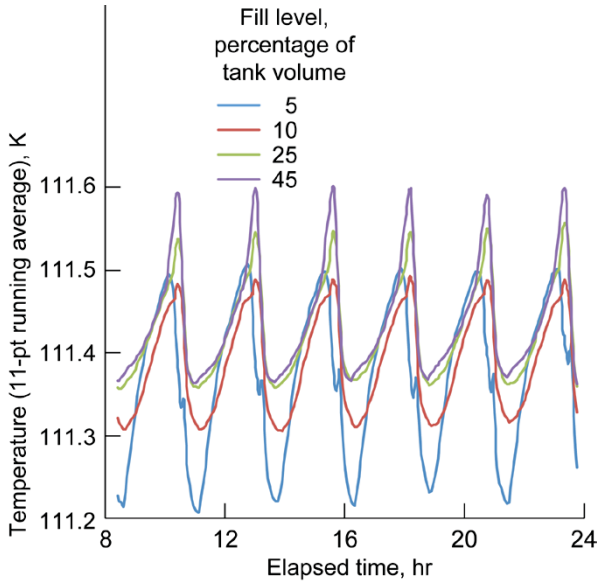

Figure 42.—Liquid temperatures during Test 50D thermodynamic vent system (TVS) cycles.

11.9 Test 50E

At the conclusion of the LO_2 test program, time was granted to conduct a single LN_2 test. The LN_2 test was performed at the nominal 50-percent fill level and a liquid temperature of 100 K. GHe pressurization was used to obtain tank pressures near 1.6 MPa, and the hardware was configured for tank mixing by the axial jet only. Figure 43 shows the pressure and liquid temperature cycles. Both temperature- and pressure-controlled tests were performed. A unique result for Test Series E was the simultaneous control of both pressure and temperature with an ullage containing GHe. Simultaneous control was demonstrated with four TVS cycles at the start followed later by another five cycles beginning at about 22 hr. During simultaneous pressure and temperature control, the TVS was operated using temperature control logic. When the TVS was venting, the test facility operator would carefully monitor the decreasing pressure. When the pressure reached a specified lower limit, the operator would manually control additional GHe flow to maintain the tank pressure at the lower limit while the TVS continued to vent and cool the liquid. When the liquid temperature reached the lower set point, the TVS venting would stop automatically and the operator would simultaneously stop adding GHe to the tank. As seen in Figure 43, both temperature and pressure remained within the control bands during these test segments. The separate temperature- and pressure-controlled segments of the test behaved very much the same as the previous LO_2 tests with GHe. When the pressure-controlled test segment ended at a lowered tank pressure (at 21 hr), GHe was added to restore the tank pressure to the initial value at the start of Test Series E.

The liquid temperatures plotted in Figure 44 look very similar to those for the other tests using the axial jet. The LN_2 test series (Test Series E) was the only one where the lid, unwetted wall,

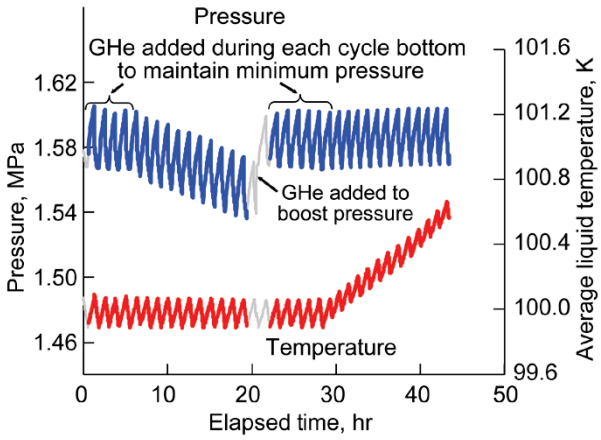

Figure 43.—Tank pressure and average liquid temperature for Test 50E; GHe, gaseous helium.

and ullage temperatures decreased as the tests progressed, as shown in Figure 45. The upper tank temperatures decreased because the tank was warm prior to filling and the tank was only filled to the 50-percent level—unlike the other 50-percent fill tests, where the tank was drained from the 90-percent level. Therefore, the upper tank continued to cool as the tests were conducted. As shown in Table III, the performance specifications for the first and third segments (the two segments with simultaneous temperature and pressure control) show some differences, such as duty cycles and vented mass. The differences are attributed to the initial unsteady thermal conditions associated with the cooling of the upper tank early in the test.

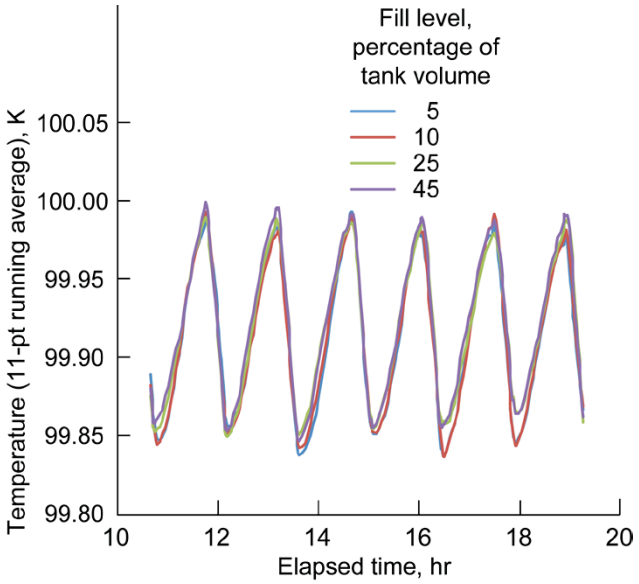

Figure 44.—Liquid temperatures during Test 50E thermodynamic vent system (TVS) cycles.

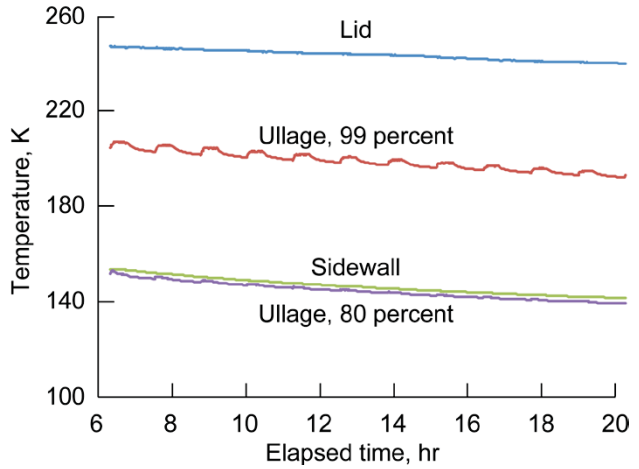

Figure 45.—Ullage, lid, and unwetted wall temperatures during Test 50E.

12.0 Observations of All Thermodynamic Vent System Test Results

The results in Tables IV and V clearly indicate better TVS performance at higher tank pressure. The heat exchanger performance is about 3 times better for Test Series B, C, and D than for Test Series A. Thus, the duty cycles are much lower for Test Series B, C, and D than for Test Series A. The improvement is due primarily to the higher vent flowrate at the higher tank pressure: the greater the vented mass, the greater the capability of the vent flow to remove energy from the tank and the lower the required heat exchanger duty cycle.

Figure 46 shows the effect of tank-to-vent pressure drop on vent flowrate. All of the LO_2 tests exhibit a common trend of increasing flowrate with pressure drop. For the same pressure drop, the vent mass flowrate of the LN_2 tests was about 25-percent lower. The volumetric flowrate in the downstream vent line where the vent gas had warmed to room temperature was approximately equal for the LO_2 tests pressurized with GHe and the LN_2 tests. The higher mass flowrate for O_2 was due primarily to its greater density. The flowrates plotted in Figure 46 are based on the flowmeter reading in the vent line.

In general, the agreement between vent flowrates determined by flowmeter readings were in good agreement with calculated values based on the tank weighing system, as shown in Figure 47. Two notable exceptions are visible in Figure 47: Tests 50E_1 and 50E_2—the first two tests performed with LN_2. The cause of the discrepancy was not determined clearly, and it is not known which of the two vent flowrate measurement methods was better. The most probable cause of error was considered to be startup transient behavior because the first and second tests had discrepancies (with the first being larger), whereas the third and fourth LN_2 tests showed good agreement. Because of the uncertainty in the LN_2 tests, the LN_2 flow vent flowrate data should be considered with caution.

The heat removal rate of the heat exchanger was proportional to the vent mass flowrate and the enthalpy change

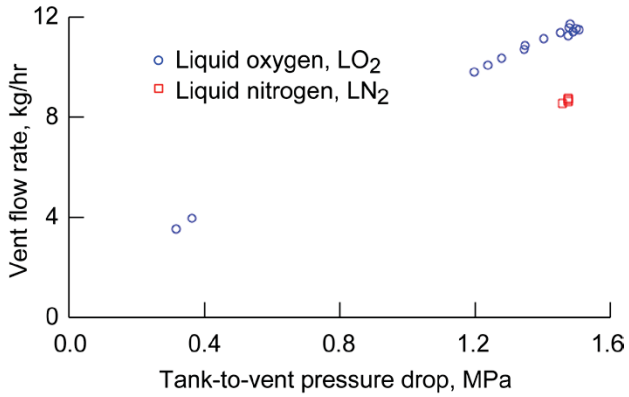

Figure 46.—Effect of pressure drop on vent flowrate.

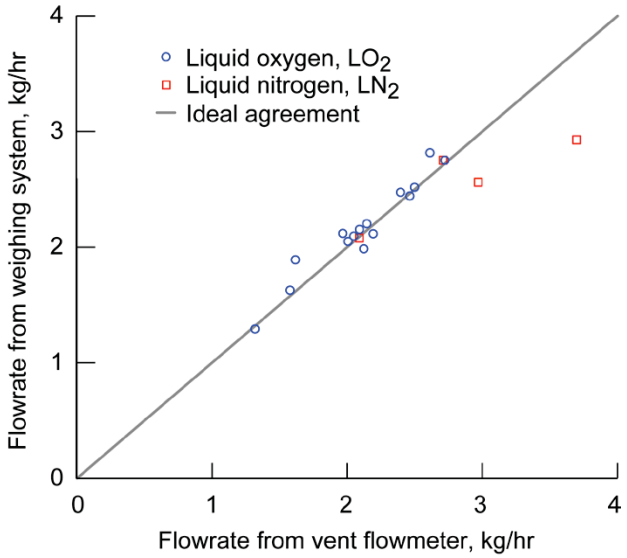

Figure 47.—Comparison of flowrates measured by vent flowmeter and tank weighing system.

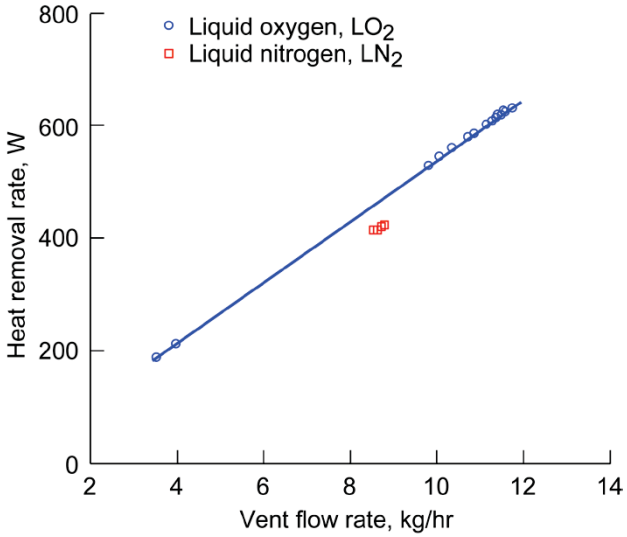

Figure 48.—Heat exchanger heat removal rate versus vent mass flowrate.

of the vented fluid, as shown in Figure 48. The data points with a heat removal rate above 500 W are for Test Series B, C, and D (LO_2 tests with GHe pressurization). The data pair near 200 W are for Test Series A (LO_2 tests without GHe pressurization). The points slightly above 400 W are for Test Series E (LN_2). The N_2 data fall below the line fitted through the O_2 data because of the lower specific enthalpy change of the vent flow across the heat exchanger for N_2 compared with O_2 (about a 10-percent difference). The quality downstream of the J–T device was 0.10 for Test Series A; 0.16 to 0.17 for Test Series B, C, and D; and 0.24 for Test Series E. The lower quality for Test Series A was a result of operating the vent system at a slightly higher back pressure than for the remainder of the test program.

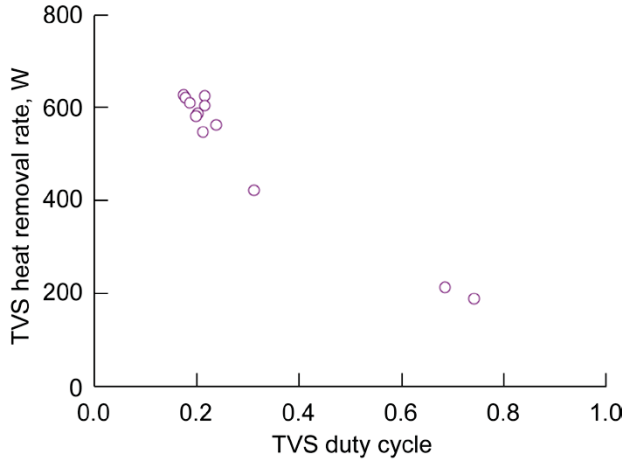

Figure 49.—Relationship between heat exchanger heat removal rate and thermodynamic vent system (TVS) duty cycle for temperature-controlled TVS operation.

Figure 49 shows the relationship between TVS heat removal rate and TVS duty cycle. Only data points for the temperature-controlled tests are shown. Close inspection of Table IV reveals that the duty cycles were always less for pressure control than for temperature control for otherwise similar test conditions (e.g., compare Tests 50B_1 and 50B_2, Tests 90C_1 and 90C_2, Tests 50C_1 and 50C_2, or Tests 50D_1 and 50D_2). Because the liquid temperature rose under pressure control, less heat was removed, thus allowing shorter duty cycles. When two sets of temperature-controlled operation were conducted, similar results were obtained for duty cycles and vented mass per cycle (e.g., Tests 50C and 50D). The sole exception was in Test 50E, which may be related to unsteady test conditions during the early part of Test Series E, as discussed in Section 11.9.

Further examination of Tables IV and V shows that the TVS performance (duty cycles, cycle-averaged vent flowrate, and heat removal rate) for a given hardware configuration was essentially the same for the high and low fill levels when temperature-controlled operation was used (e.g., Test Series A, B, C, and D). No significant effects of fill level were found.

There was a subtle difference in performance for the various hardware configurations. The combined axial jet and spray hoops configuration had the largest TVS duty cycles and time-averaged vent flowrates. All the data were carefully examined, and no attributable differences in vacuum level, vacuum chamber wall temperature, or other environmental variables were found. With the combined mode used as the basis for comparison, for the axial jet, the TVS duty cycle was about 16-percent lower and the time-averaged vented mass was about 14-percent lower. The time-averaged vented mass was expected to be less for the axial jet configuration because the temperature of the unwetted tank wall, lid, and ullage were not controlled with an axial jet in the 1g environment. In all the LO_2 axial jet tests, these temperatures were increasing with

time; thus not all the tank's energy input was removed and the vented mass was less than if complete temperature control had occurred.

Similarly, when the performance of the spray-hoops-only configuration was compared with that of the combined mode, the TVS duty cycle was about 13-percent lower and the time-averaged vented mass was about 14-percent lower. However, the difference is not due to thermal control of the upper tank region because temperatures here exhibited essentially identical behavior for these two configurations. The most probable explanation is incomplete mixing and thermal control of the liquid during operation of the spray-hoops-only configuration. The apparently successful operation of the TVS with the spray-hoops-only configuration was somewhat surprising. The high heat input rate for the tests may have promoted rather vigorous free convection within the test tank. Perhaps the free convection provided partial mixing while not achieving isothermal liquid temperatures.

When the overall energy balance was applied to the results, the average pump power dissipation was 75 W for the axial jet (Test Series B), 160 W for the combined axial jet and spray hoops (Test Series C), and 85 W for the spray-hoops-only configuration (Test Series D). There is no cause for the actual power dissipation to vary for these test series. The value for the combined mode is probably the closest to the true value because the combined mode represents the most likely of the three test series to be at uniform thermal conditions, as assumed in the model. For Test Series B, the missing thermal energy increase was probably storage in the upper tank region; whereas for Test Series D, the missing amount could have been the thermal energy increase in the liquid (due to incomplete mixing/cooling) that was not observed directly.

For the LO_2 tests using temperature control, Table V provides additional performance metrics. The turnover time, computed from Equation (35) is listed, as well as the pump-on time (equal to $\lambda_p t_{\text{cycle}}$). The ratio of pump-on time to turnover time is also provided. One observation is that the ratio was much greater than unity for Test Series A; this is due to (1) the reduced performance of the heat exchanger resulting from the lower vent flowrate and (2) the larger control band for temperature. Note that, for a fair comparison, the ratio of pump-on time to turnover time should only be compared for tests using the same control bands because using a wider control band increases the pump-on time. For Test Series B to E (all with temperature-control bandwidths of 0.17 K), the ratio of pump-on time to turnover time was roughly equal to 1, ranging from 0.7 to 1.4. Therefore, the combined mixing and cooling process may be viewed as largely due to the action of pumping the entire liquid volume through the heat exchanger. The ratio of pump-on time to turnover time was lower at the high fill-level tests than at the lower fill-level tests. The reason for fill-level dependence is not known. One thought is there may have been a significant time delay in the startup performance of the heat exchanger. The delay would have a greater impact on the low fill-level tests where the turnover time was shorter.

The axial jet configuration was most efficient, with ratios significantly less than 1, an indicator that the bulk liquid was well mixed by the jet flow. The ratios were larger for Test Series C and D (combined mode and spray hoops) than for Test Series B (axial jet) because some or all of the mixing flow was routed through the spray hoops. The liquid droplets impinging on the unwetted tank wall and lid absorbed heat before falling to the liquid surface. The thermal energy gain of the falling droplets was added to the liquid; thus, longer TVS and pump-on time were required.

The uncertainty estimates provided in Tables IV and V show typical values of 0.1 to 0.4 percent for the cycle time, 0.01 for the duty cycle, 4 to 5 percent for the vent mass and vent flowrate, and 4 to 5 percent for the heat removal rate. The exception is Test Series 50B, where larger uncertainties resulted from a slower than desired data-recording rate. The recording rate was similar to those for the other LO_2 test series (Test Series A, C, and D), but the significantly shorter cycle times for Test Series 50B led to larger uncertainties in the computed performance metrics.

The dissipated pump power calculated from the energy balance (Eq. (41)) for the temperature-controlled test segments was reasonably consistent for axial jet (Test Series A and B), spray-hoops-only (Test Series D), and combined axial jet and spray hoops operation (Test Series C). The combined mode had the highest calculated value (average of all pertinent test segments) of 159 W, which the author considered to be the most correct value for the pump power because the tank conditions are thought to be mostly isothermal as assumed in the energy balance analysis. The value for the axial jet tests was 75 W; a value that is probably reduced because of the energy stored in the tank lid and unwetted wall. (Lid and unwetted wall temperatures increased during the axial jet tests.) The value for the spray-hoops-only tests was 84 W and is an indication of energy storage somewhere in the system. A likely explanation is that the storage was in the liquid because the liquid may not have been well mixed with spray hoops circulation only. The energy balance method was not applied to the LN_2 tests (Test Series E) because a boiloff test was not conducted with LN_2 and the tank heating rate (when filled with LN_2) was unknown.

The last column in Table V gives the TVS efficiency based on Equation (42). To make the comparison more "fair," an adjusted boiloff flowrate was calculated assuming that the second and third terms on the right-hand side of Equation (32) were equal to zero for the same tank heating rate. The resulting boiloff flowrates for the LO_2 tests were 1.85 to 1.87 kg/hr. TVS efficiencies were computed only for temperature-controlled tests. The efficiency was poorest for Test Series A. The author attributes this to the inefficient heat

exchanger performance at the off-design operating condition (low tank pressure) and the resulting high pump/TVS duty cycles, where an increased amount of pump energy was dissipated into the tank. Much improved efficiencies for the axial jet configuration were obtained in Test Series B. The higher efficiency at the lower fill level was probably due to greater unwetted wall heating (less energy removed by the TVS). The efficiencies for Test Series C (combined mode) were not as good as for Test Series B (axial jet). The lower efficiency for Test Series C was due to the compete cooling of the entire tank and contents and the greater amount of energy removal. Test Series D (combined mode) had better efficiency than Test Series C. The Test Series C to Test Series D efficiency comparison may be misleading if the liquid was not well mixed by the spray-hoops-only configuration as speculated.

13.0 Comparison of Test Results With Thermodynamic Vent System Model

Results from several test sets were selected for comparison with the model presented in Section 1.2. Test Series C was selected because the combined use of the axial jet and the spray hoops provided the best assurance that the tank contents were isothermal as the model assumes. The pressure data for the first temperature-controlled set from Test 90C (~90-percent fill) is shown in Figure 50 along with the predicted minimum pressures for each cycle. The model input parameters were the initial pressure, initial fill level, temperature (constant), pump duty cycle, environmental heat input rate, and the pump power dissipation rate. The agreement between the model and experimental results is quite good, with the model predicting a slightly faster rate of pressure drop. In Figure 51, the next portion from Test 90C is shown. Here, the pressure was kept constant, causing the temperature to rise. The model predicted a slightly lower temperature rise rate, but again the agreement with the data was quite good.

Similar comparisons of the model predictions with the experimental results from Test 50C (~50-percent fill) are shown in Figure 52 for a temperature-controlled segment and in Figure 53 for a pressure-controlled segment. The agreement is very good for both cases. Again, all values input to the model were matched to the test values.

The last comparison was for the nitrogen Test 50E (axial jet, ~50-percent fill) using combined pressure and temperature control. Figure 54 shows the experimental fill levels for the third test segment plotted against the predicted values. The agreement is good. Also shown is the predicted amount of added helium as a percentage of the initial helium mass. The quantity of added helium was not measured in the tests. The amount added was small, about 0.7-percent of the initial mass was required for each TVS cycle.

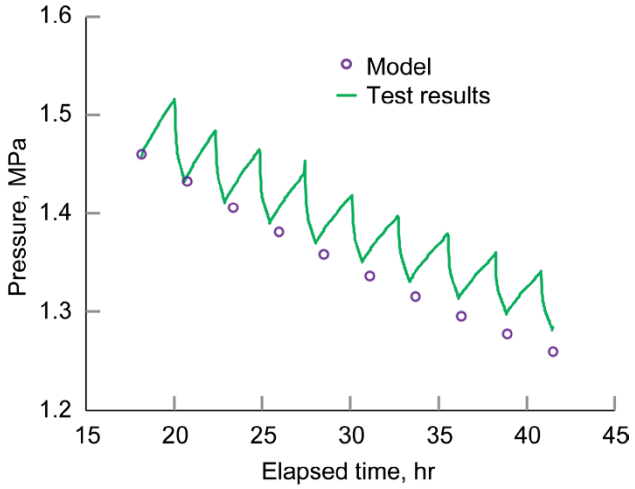

Figure 50.—Comparison of model predictions with data at 90-percent fill with temperature control.

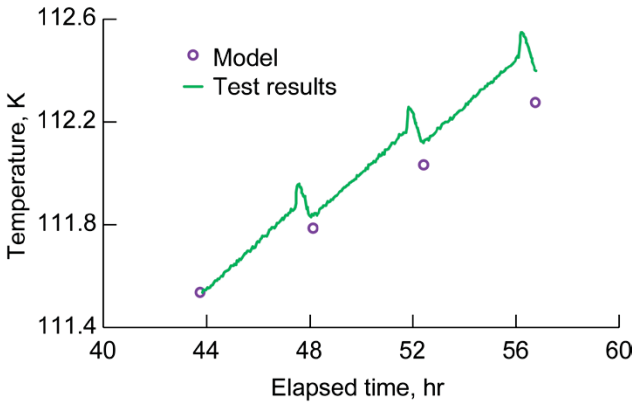

Figure 51.—Comparison of model predictions with data at 90-percent fill with pressure control.

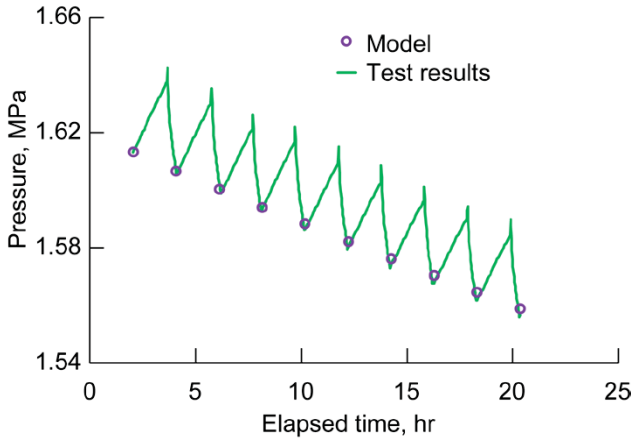

Figure 52.—Comparison of model predictions with data at 50-percent fill with temperature control.

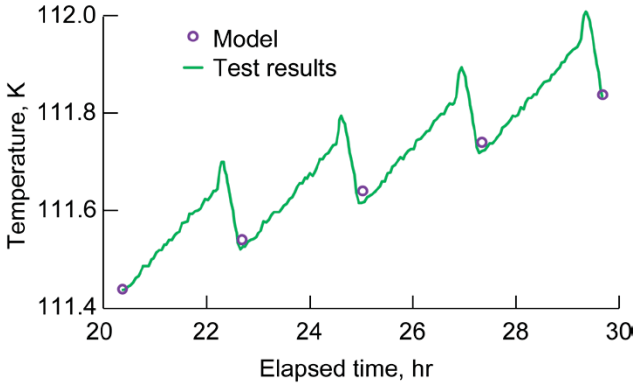

Figure 53.—Comparison of model predictions with data at 50-percent fill with pressure control.

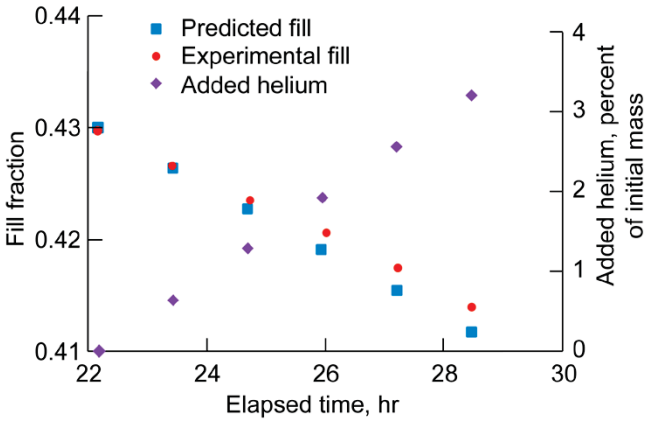

Figure 54.—Comparison of model predictions with data at 50-percent fill with systematic helium addition.

14.0 Conclusions

An active thermodynamic vent system (TVS) was successfully demonstrated in a liquid oxygen tank pressurized with helium. Tests were conducted at nominal fill levels of 90 and 50 percent. The liquid was heated above its normal boiling point to represent thermodynamic conditions in a candidate lunar lander ascent stage. Three different hardware configurations for mixing the cooled liquid with the bulk fluid were tested: a submerged axial jet, a pair of spray hoops in the ullage, and combined operation of both. The combined mode maintained temperature throughout the entire tank, whereas the axial jet maintained liquid temperatures but did not control ullage temperatures. The spray-hoops-only mode was generally able to maintain liquid temperatures, although one test set was not successful. The liquid mixing may have been assisted by free convection driven by the high heat leak into the test tank. An initial test without helium pressurization verified the expected TVS behavior for the pure liquid and vapor condition in which the liquid temperature was controlled when the TVS was used to maintain tank pressure within a specified band.

The presence of helium in the ullage decoupled the tank pressure from the liquid temperature. The experimental results showed that if the tank pressure was kept within a control band, the liquid temperature rose with each successive TVS cycle. Similarly, if the temperature was kept within a control band, the tank pressure would drop with each successive TVS cycle. A simple thermodynamic model was developed that predicts these trends. Correlation of modeling results shows that the amount of temperature rise or pressure drop per cycle was proportional to both the helium mole fraction and the heat input into the tank. The tank fill level was also important because the amount of temperature rise or pressure drop per TVS cycle increased as the ullage volume decreased.

An additional test with liquid nitrogen pressurized with helium was conducted to demonstrate that simultaneous control of pressure and liquid temperature was possible by systematic introduction of a small amount of helium during each TVS cycle. The added helium occupied the volume of liquid removed from the tank during TVS venting cycles and existed as part of a binary ullage mixture along with propellant vapor.

Glenn Research Center
National Aeronautics and Space Administration
Cleveland, Ohio, April 24, 2014

Appendix—Symbols

C	flowmeter coefficient
CntrlFlg	flag for user-specified choice of temperature- or pressure-control logic
DPDT	user-specified tank pressure decay rate in control logic
F	liquid fill fraction
GHe	gaseous helium
h	enthalpy
id	propellant identification (e.g., “oxygen” or “methane”)
LCH_4	liquid methane
LH_2	liquid hydrogen
LN_2	liquid nitrogen
LO_2	liquid oxygen
m	mass
$\overline{m}$	averaged mass
$\dot{m}$	mass flowrate
$\overline{\dot{m}}$	averaged mass flowrate
N_2	nitrogen
O_2	oxygen
P	pressure
Q	heat/energy transfer
$\dot{Q}$	heat input rate
$\overline{\dot{Q}}$	averaged heat input rate
R	individual load cell (weighing system) reading
T	temperature
t	time
$\bar{t}$	averaged time
U	total internal energy or uncertainty
u	specific internal energy
V	volume
x	fluid quality (mass fraction of vapor)
α	first coefficient in weighing system calibration equation
β	second coefficient in weighing system calibration equation
γ	third coefficient in weighing system calibration equation
ζ	constant in smoothing function for rate of change of pressure
η	efficiency
λ	duty cycle
ρ	density
τ	tank turnover time
ϕ	energy derivative defined in Equation (33)
Ω	volumetric flowrate

Subscripts

cal	flowmeter calibration
cp	critical point
cycle	single thermodynamic vent system cycle
e	environmental
*el*0	elapsed time control logic for checking maximum temperature or pressure
*el*1	elapsed time control logic for checking rate of pressure decay
*el*2	elapsed time control logic for checking minimum temperature or pressure
ex	exit
f	saturated liquid
fin	final
fl	fluid
fluid	flowmeter fluid conversion
fm	flowmeter
g	saturated vapor
He	helium
HX	heat exchanger
in	inlet of heat exchanger or Joule-Thomson device
int	initial

j	load cell identification number (1 to 3)
ℓ	liquid
lc	load cell
min	minimum
max	maximum
new	value at current time step during data acquisition
o	out (via venting or boiloff)
old	value from previous time step during data acquisition
out	outlet of heat exchanger
p	pump
ref	reference
sat	saturated
TVS	thermodynamic vent system
tp	triple point
u	ullage
v	vapor
vent	thermodynamic vent system vent
1	initial state
2	final state

Superscripts

*	dimensionless quantity in correlation
†	dimensionless quantity in correlation
‡	derived from mass balance
◊	derived from energy balance

Acronyms

J–T	Joule-Thomson
MLI	multilayer insulation
TVS	thermodynamic vent system

References

1. Flachbart, R.H.; Hastings, L.J.; and Martin, J.J.: Testing of a Spray Bar Zero Gravity Cryogenic Vent System for Upper Stages. AIAA paper 99–2175, 1999.
2. Hastings, L.J., et al.: Spray Bar Zero-Gravity Vent System for On-Orbit Liquid Hydrogen Storage. NASA/TM—2003-212926, 2003. http://ntrs.nasa.gov
3. Flachbart, R.H., et al.: Testing of a Spray-Bar Thermodynamic Vent System in Liquid Nitrogen. Advances Cryogenic Engineering, J.G. Weisend II, ed., vol. 823, 2006, pp. 240–247.
4. Flachbart, R.H., et al.: Thermodynamic Vent System Performance Testing With Subcooled Liquid Methane and Gaseous Helium Pressurant. Cryogenics, vol. 48, issues 5–6, 2008, pp. 217–222.
5. Flachbart, R.H., et al.: Testing the Effects of Helium Pressurant on Thermodynamic Vent System Performance With Liquid Hydrogen. Advances Cryogenic Engineering, J.G. Weisend II, ed., vol. 985, 2008, pp. 1483–1490.
6. VanOverbeke, T.J.: Thermodynamic Vent System Test in a Low Earth Orbit Simulation. NASA/TM—2004-213193, 2004. http://ntrs.nasa.gov
7. Aydelott, J.C.: Modeling of Space Vehicle Propellant Mixing. NASA TP–2107, 1983. http://ntrs.nasa.gov
8. Bentz, M.D.; Knoll, R.H.; and Lin, C.S.: Low-G Fluid Mixing: Further Results From the Tank Pressure Control Experiment. AIAA–93–2423, 1993.
9. Papell, S. Stephen; Saiyed, Naseem H.; and Nyland, Ted W.: Acquisition and Correlation of Cryogenic Nitrogen Mass Flow Data Through a Multiple Orifice Joule-Thomson Device. NASA TM–103121, 1990. http://ntrs.nasa.gov
10. Papell, S. Stephen; Nyland, Ted W.; and Saiyed, Naseem H.: Liquid Hydrogen Mass Flow Through a Multiple Orifice Joule-Thomson Device. NASA TM–105583, 1992. http://ntrs.nasa.gov
11. Jurns, John M.: Visco Jet Joule-Thomson Device Characterization Tests in Liquid Methane. NASA/CR—2009-215497, 2009. http://ntrs.nasa.gov
12. Lemmon, Eric W.; Huber, Marcia L.; and McLinden, Mark O.: NIST Standard Reference Database 23: NIST Reference Fluid Thermodynamic and Transport Properties—REFPROP, Version 8.0, National Institute of Standards and Technology, Standard Reference Data Program, Gaithersburg, MD, 2007.
13. Zimmerli, Gregory A.; Asipauskas, Marius; and Van Dresar, Neil T.: Empirical Correlations for the Solubility of Pressurant Gases in Cryogenic Propellants. Cryogenics, vol. 50, issue 9, 2010, pp. 556–560.
14. Christie, Robert J.: Two-Phase Cryogenic Heat Exchanger for the Thermodynamic Vent System. NASA/TM—2011-217220, 2011. http://ntrs.nasa.gov
15. Electro-Fluidic Systems Handbook: RELEASE 8—Component Catalog with engineering reference material. The Lee Company Technical Center, Westbrook, CT. http://www.theleeco.com/pdf/Lee_EFS_Handbook_8thEdition.pdf Accessed Feb. 2014.
16. Lin, Chin S.; Van Dresar, Neil T.; and Hasan, Mohammad M.: Pressure Control Analysis of Cryogenic Storage Systems. J. Propul. Power, vol. 20, no. 3, 2004, pp. 480–485.
17. Coleman, Hugh W.; and Steele, W. Glenn, Jr.: Experimentation and Uncertainty Analysis for Engineers. Second ed., Wiley, New York, NY, 1999.
18. Christie, R.J.: NASA Glenn Research Center, 2011, personal communication (author of Ref. 14).